

# $O(k)$ -Equivariant Dimensionality Reduction on Stiefel Manifolds

Andrew Lee\*, Harlin Lee†, Jose A. Perea‡, Nikolas Schonscheck§, and Madeleine Weinstein¶

**Abstract.** Many real-world datasets live on high-dimensional Stiefel and Grassmannian manifolds,  $V_k(\mathbb{R}^N)$  and  $Gr(k, \mathbb{R}^N)$  respectively, and benefit from projection onto lower-dimensional Stiefel (respectively, Grassmannian) manifolds. In this work, we propose an algorithm called *Principal Stiefel Coordinates (PSC)* to reduce data dimensionality from  $V_k(\mathbb{R}^N)$  to  $V_k(\mathbb{R}^n)$  in an  $O(k)$ -equivariant manner ( $k \leq n \ll N$ ). We begin by observing that each element  $\alpha \in V_n(\mathbb{R}^N)$  defines an isometric embedding of  $V_k(\mathbb{R}^n)$  into  $V_k(\mathbb{R}^N)$ . Next, we optimize for such an embedding map that minimizes data fit error by warm-starting with the output of principal component analysis (PCA) and applying gradient descent. Then, we define a continuous and  $O(k)$ -equivariant map  $\pi_\alpha$  that acts as a “closest point operator” to project the data onto the image of  $V_k(\mathbb{R}^n)$  in  $V_k(\mathbb{R}^N)$  under the embedding determined by  $\alpha$ , while minimizing distortion. Because this dimensionality reduction is  $O(k)$ -equivariant, these results extend to Grassmannian manifolds as well. Lastly, we show that the PCA output globally minimizes projection error in a noiseless setting, but that our algorithm achieves a meaningfully different and improved outcome when the data does not lie exactly on the image of a linearly embedded lower-dimensional Stiefel manifold as above. Multiple numerical experiments using synthetic and real-world data are performed.

**Key words.** Dimensionality reduction, Equivariance, Stiefel manifold, Grassmannian manifold, Manifold learning, Principal component analysis

**MSC codes.** 55-08, 68W99, 53Z50

**1. Introduction.** Stiefel manifolds are a natural setting for data sets appearing in a wide variety of disciplines, including image processing [35], sensor array processing [27], bioinformatics [33], and astronomy [16]. In recent years, there has been broad interest in dimensionality reduction methods for manifold-valued data, e.g. [3, 15, 37]. The work of [24] introduced Principal Projective Component Analysis, an adaptation of Principal Component Analysis (PCA) to the settings where  $O(1)$  acts on  $V_1(\mathbb{R}^n)$  by scalar multiplication (with quotient equal to the real projective space  $\mathbb{R}P^{n-1}$ ) and where the unitary group  $U(1)$  acts on  $V_1(\mathbb{C}^n)$  via scalar multiplication (with quotient equal to the complex projective space  $\mathbb{C}P^{n-1}$ ). In a similar vein, [26] introduced Lens PCA, a modification of PCA suitable for lens spaces, which are the quotient spaces corresponding to the action of  $\mathbb{Z}_q$  on  $V_1(\mathbb{C}^n)$  given by scalar multiplication by powers of a primitive  $q$ -th root of unity. Generalizing methods such as PCA or multidimensional scaling to non-Euclidean spaces brings familiar tools to bear on these problems, while also incorporating information contained in the underlying geometry and topology of the data. In this article, we build on previous works by introducing a dimensionality reduction method suitable for all real Stiefel manifolds.

A key feature of Stiefel manifolds is their symmetry with respect to the action of the

\*St. Thomas Aquinas College, Sparkill, NY (alee@stac.edu).

†University of North Carolina at Chapel Hill, Chapel Hill, NC (harlin@unc.edu).

‡Northeastern University, Boston, MA (j.pereabenitez@northeastern.edu).

§University of Delaware, Newark, DE (nischon@udel.edu). Corresponding author.

¶University of Puget Sound, Tacoma, WA (mweinstein@pugetsound.edu).

orthogonal group, the quotient by which is a Grassmannian manifold. In order to produce a representation of the data that respects the symmetry of the underlying space, it is essential to perform dimensionality reduction in an *equivariant* manner. That is, let  $\mathbb{F} = \mathbb{R}$  or  $\mathbb{C}$ , and let  $V_k(\mathbb{F}^N)$  be the Stiefel manifold of  $k$ -planes in  $\mathbb{F}^N$ . Let  $G$  be a group that acts on  $V_k(\mathbb{F}^N)$ . In this work, we describe a technique (see Algorithm 1.1) that produces an optimal projection  $\pi : \mathcal{Y} \mapsto \tilde{\mathcal{Y}} \subset V_k(\mathbb{R}^n)$ , for  $n < N$  such that  $\pi(x \cdot g) = \pi(x) \cdot g$  for  $x \in X$  and  $g \in G$ . Because our methodology respects the orthogonal group action on Stiefel manifolds, i.e., is equivariant, Algorithm 1.1 can also be adapted to handle data living on Grassmannian manifolds, as detailed in Algorithm 1.2.

This equivariance property of our projection map is a key feature not generally present in similar dimensionality reduction methods. While [11] produces embeddings of hyperbolic spaces equivariant with respect to the Lorentz group action, this seems to be a relatively recent development. The method of principal nested shape spaces in [9] works with Kendall’s shape spaces, which are quotients of spheres by the action of orthogonal groups. However, their approach is not to construct an equivariant projection, but rather to consider only the subset of the so-called pre-shape sphere on which the projection map is a bijection.

**1.1. Contributions and paper outline.** Here, we summarize the contributions of this work.

1. Algorithmically, we establish a dimensionality reduction algorithm, *Principal Stiefel Coordinates (PSC)*, specifically for data living on Stiefel manifolds. Since our algorithm is  $O(k)$ -equivariant and data on Grassmanian manifolds can be easily lifted to and processed in Stiefel manifolds, our algorithm can be applied to a broader set of data compared to prior work on Grassmanian manifolds.
2. Theoretically, we define a projection map  $\pi_\alpha$  that maps data on a high-dimensional Stiefel manifold onto the image of an embedded low-dimensional Stiefel manifold, and prove its continuity and  $O(k)$ -equivariance. Furthermore, we show that when data lies *exactly* on a lower-dimensional space, the output of PCA leads to a mapping  $\alpha$  that *globally* minimizes the projection error despite it being a non-convex optimization problem. However, PCA may not be the best choice when the data does not follow the strict low-dimensionality assumption. In these cases, we demonstrate how an additional gradient descent step results in an improved outcome.
3. Experimentally, we demonstrate PSC on both low-dimensional and high-dimensional simulation data, as well as real brain connectivity matrices and simulated neuronal stimulus space model data. We compare our results to existing methods such as PCA, multidimensional scaling (MDS), persistent cohomology, and principal geodesic analysis (PGA). Our Python code is available publicly on Github.

In Section 2, we specify our notation and provide background information on Stiefel manifolds, singular value decomposition, polar decomposition, and equivariance. In Section 3, we define the projection map  $\pi_\alpha$  and prove that it is continuous (Theorem 3.7), equivariant (Proposition 3.8), and minimizes distortion of the data (Propositions 3.9 and 3.10). In Section 4, we describe our process for optimizing the projection map and prove that when the data lies exactly on a lower-dimensional space, the output of PCA leads to a mapping that globally minimizes the projection error (Theorem 4.5). In Section 5, we test our algorithm on various

data sets.

**1.2. Main algorithm pipelines.** To outline the main mathematical contents of the paper, we summarize below the essential steps in our dimensionality reduction pipeline. While we freely use notation that will be defined later in the paper, we hope the following will be a useful reference for the reader.

---

**Algorithm 1.1** Principal Stiefel Coordinates (PSC): Dimensionality reduction for Stiefel manifolds

---

- 1: Suppose as given a data set  $\mathcal{Y} \subset V_k(\mathbb{R}^N)$ .
- 2: Fix a user-chosen target dimension  $n \ll N$  for the dimensionality reduction.
- 3: For any  $\alpha \in V_n(\mathbb{R}^N)$ , note that  $\alpha$  defines an isometric embedding  $V_k(\mathbb{R}^n) \xrightarrow{\alpha} V_k(\mathbb{R}^N)$ ; see left-hand side of Figure 1.1 and Proposition 3.3. Let  $\pi_\alpha: T \rightarrow \text{im}(\alpha)$  be the continuous, distance-minimizing, equivariant projection defined on a neighborhood  $T$  of radius  $\sqrt{2}$  about  $\text{im}(\alpha)$  constructed in Section 3.
- 4: Construct  $\alpha_{PCA} \in V_n(\mathbb{R}^N)$  as in Section 4.1, which will serve as the initialization for an optimization problem on  $V_n(\mathbb{R}^N)$ .
- 5: Perform gradient descent on  $V_n(\mathbb{R}^N)$  to find

$$(1.1) \quad \alpha_{GD} := \operatorname{argmin}_{\alpha \in V_n(\mathbb{R}^N)} \frac{1}{|\mathcal{Y}|} \sum_{y \in \mathcal{Y}} \|y - \pi_\alpha(y)\|^2$$

using  $\alpha_{PCA}$  as the initialization.

- 6: For each  $y \in \mathcal{Y}$ , consider the point  $\pi_{\alpha_{GD}}(y) = \alpha_{GD}(\hat{y}_{\alpha_{GD}})$  as detailed in Definition 3.4. Let  $\pi_{\alpha_{GD}}(\mathcal{Y})$  be the set  $\{\pi_{\alpha_{GD}}(y) \mid y \in \mathcal{Y}\} \subset V_k(\mathbb{R}^n)$ .
  - 7: Obtain the representation  $\pi_{\alpha_{GD}}(\mathcal{Y}) \subset \alpha_{GD}(V_k(\mathbb{R}^n))$  of the data  $\mathcal{Y}$  as a subset of the isometric image of  $V_k(\mathbb{R}^n)$  under  $\alpha_{GD}$ .
- 

It is worth noting that from an implementation perspective, the image of a data point  $y \in \mathcal{Y}$  under our dimensionality reduction pipeline is the point  $\hat{y}_{\alpha_{GD}} \in V_k(\mathbb{R}^n)$  as in Step 6. That is, to recover data living on  $V_k(\mathbb{R}^n)$  from Algorithm 1.1, one would apply the left inverse  $\alpha_{GD}^\top$  of  $\alpha_{GD}$  to  $\pi_{\alpha_{GD}}(\mathcal{Y})$ , which simply recovers  $\hat{y}_{\alpha_{GD}}$ . Indeed, for any  $y \in \mathcal{Y}$ , we have

$$(1.2) \quad \alpha_{GD}^\top \pi_{\alpha_{GD}}(y) = \alpha_{GD}^\top \alpha_{GD}(\hat{y}_{\alpha_{GD}}) = \hat{y}_{\alpha_{GD}}.$$

However, from a conceptual standpoint, we find it useful to think of our pipeline as 1) embedding  $V_k(\mathbb{R}^n)$  in  $V_k(\mathbb{R}^N)$  via  $\alpha_{GD}$ , then 2) performing a projection from  $V_k(\mathbb{R}^N)$  to  $\alpha_{GD}(V_k(\mathbb{R}^n))$ , and finally 3) “pulling back” to data in  $V_k(\mathbb{R}^n)$ . Moreover, the gradient descent in Step 5 uses the projected points  $\pi_\alpha(y) \in V_k(\mathbb{R}^n)$  in an essential way. The right-hand side of Figure 1.1 gives an overview of our pipeline.

Because Algorithm 1.1 uses an equivariant projection  $\pi_{\alpha_{GD}}$ , our technique can also be applied to data living on Grassmannian manifolds  $Gr(k, \mathbb{R}^N)$ . In further detail, for any  $y \in V_k(\mathbb{R}^N)$  and  $g \in O(k)$ , it follows from Proposition 3.8 that  $\pi_{\alpha_{GD}}(y)g = \pi_{\alpha_{GD}}(yg)$ . Hence, we have that

$$(1.3) \quad \alpha_{GD}^\top \pi_{\alpha_{GD}}(y)g = \alpha_{GD}^\top \pi_{\alpha_{GD}}(yg).$$

This shows that the algorithm below is well-defined.

---

**Algorithm 1.2** Dimensionality reduction for Grassmannian manifolds

---

- 1: Suppose as given a data set  $\bar{\mathcal{Y}} \subset Gr(k, \mathbb{R}^N)$ .
  - 2: For each  $\bar{y} \in \bar{\mathcal{Y}}$ , choose an orthonormal basis of  $\bar{y}$  to obtain an associated point  $y \in V_k(\mathbb{R}^n)$ , and let  $\mathcal{Y} = \{y \mid \bar{y} \in \bar{\mathcal{Y}}\}$ . Note that any two orthonormal bases  $y$  and  $y'$  are related by an element of  $O(k)$ . That is,  $y' = yg$  for some  $g \in O(k)$ .
  - 3: Perform Algorithm 1.1 on the set  $\mathcal{Y}$  to obtain  $\mathcal{X} \subset V_k(\mathbb{R}^n)$ .
  - 4: Project  $\mathcal{X} \subset V_k(\mathbb{R}^n)$  to  $Gr(k, \mathbb{R}^n)$  via the canonical quotient map  $V_k(\mathbb{R}^n) \rightarrow Gr(k, \mathbb{R}^n)$  to obtain the set  $\bar{\mathcal{X}} \subset Gr(k, \mathbb{R}^n)$ .
  - 5: Recover a representation  $\bar{\mathcal{X}}$  of the original data as a subset of  $Gr(k, \mathbb{R}^n)$ .
- 

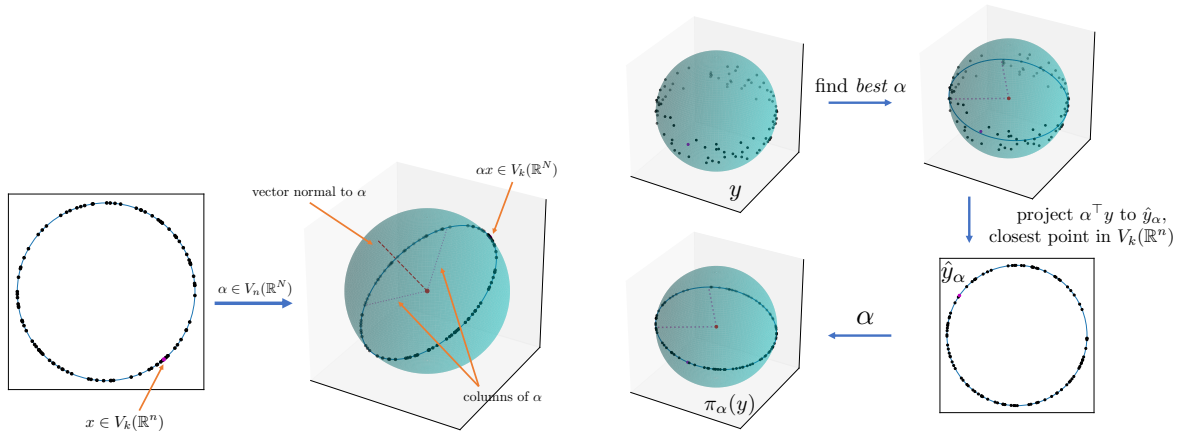


**Figure 1.1.** Left:  $\alpha \in V_n(\mathbb{R}^N)$  defines an isometric embedding from  $V_k(\mathbb{R}^n)$  to  $V_k(\mathbb{R}^N)$ , as illustrated here in  $k = 1, n = 2, N = 3$ . Right: Outline of Principal Stiefel Coordinates (PSC) Algorithm 1.1 illustrated with  $k = 1, n = 2, N = 3$ .  $y, \pi_\alpha(y) \in V_k(\mathbb{R}^N), \alpha \in V_n(\mathbb{R}^N), \hat{y}_\alpha \in V_k(\mathbb{R}^n)$ .

**2. Preliminaries.** This section is devoted to fixing notation and summarizing standard results that will be used throughout the rest of the paper. For a handy reference, Table 2.1 details our most commonly used notation.

**2.1. Notations.** The notation  $\mathbb{R}^{s \times t}$  denotes an  $s \times t$  matrix with entries in  $\mathbb{R}$ ,  $I_s$  an  $s \times s$  identity matrix, and  $0_{s \times t}$  an all-zero matrix of size  $s \times t$ . We use  $A^\top$  and  $A^*$  to denote the transpose and hermitian of the matrix  $A$ , respectively. The trace of  $A$  is  $\text{tr}(A)$ ,  $\|A\|_F$  is the Frobenius norm of  $A$ , and  $\|A\|_{op}$  is the operator norm, i.e. the largest singular value. Lastly,  $|S|$  is the cardinality of the set  $S$ , and  $\text{im}(A)$  is the image of  $A$ . See Table 2.1 for more.

**2.2. Stiefel manifolds.** For the following definitions, we use arbitrary dimensions  $0 < t < s$ .

**Definition 2.1 (Stiefel manifold).** The **Stiefel manifold**  $V_t(\mathbb{R}^s)$  is the set of orthonormal  $t$ -frames in  $\mathbb{R}^s$ . That is, an element in  $V_t(\mathbb{R}^s)$  is an ordered set of  $t$  orthonormal vectors in  $\mathbb{R}^s$ .

Notation	Meaning
$k, n, N$	Data dimensions $0 < k \leq n \ll N$ .
$V_t(\mathbb{R}^s)$	Stiefel manifold of orthonormal $t$ -frames in $\mathbb{R}^s$ (c.f. 2.1).
$Gr(t, \mathbb{R}^s)$	Grassmanian manifold of $t$ -dimensional subspaces in $\mathbb{R}^s$ .
$O(t)$	Orthogonal group in $\mathbb{R}^t$ .
$x, \mathcal{X}$	Data points on $V_k(\mathbb{R}^n)$ , $x \in \mathcal{X}$ .
$y, \mathcal{Y}$	Data points on $V_k(\mathbb{R}^N)$ , $y \in \mathcal{Y}$ .
$\alpha$	A point in $V_n(\mathbb{R}^N)$ (c.f. 3.3).
$\alpha_{PCA}$	The warm-start embedding used in Step 4 of Algorithm 1.1.
$\alpha_{GD}$	The embedding produced through gradient descent on $V_n(\mathbb{R}^N)$ (c.f. Step 5 of Algorithm 1.1).
$\pi_\alpha$	A projection map from a suitable subset of $V_k(\mathbb{R}^N)$ to $\alpha(V_k(\mathbb{R}^n))$ (c.f. 3.4).
$\hat{y}_\alpha$	A point on $V_k(\mathbb{R}^n)$ that is closest to $\alpha^\top y$ (c.f. 3.4).

**Table 2.1**

Frequently referenced notations.

The  $V_t(\mathbb{R}^s)$  Stiefel manifolds are by definition embedded in the Euclidean space of matrices  $\mathbb{R}^{s \times t}$ .

**Proposition 2.2.** *An  $s \times t$  matrix  $A$  is in  $V_t(\mathbb{R}^s)$  if and only if  $A^\top A = I_t$ .*

*Proof.* The entries of the product  $A^\top A$  consist of the pairwise inner products of the  $t$  columns of  $A$ , which are orthonormal by assumption. ■

Each Stiefel manifold comes equipped with several choices of distance function. We inherit the following distance from the ambient space of matrices.

**Definition 2.3.** *For  $P, Q \in \mathbb{R}^{s \times t}$ , define*

$$(2.1) \quad D(P, Q) = \|P - Q\|_F = \sqrt{\left( \sum_{i=1}^s \sum_{j=1}^t (P[i, j] - Q[i, j])^2 \right)}$$

*This norm is induced by an inner product on the ambient space of matrices:*

$$(2.2) \quad \langle P, Q \rangle_D = \text{tr}(P^\top Q).$$

We will also refer to the following norm on matrices.

**Definition 2.4 (Nuclear norm).** *We denote the **nuclear norm** of a matrix  $A$  as  $\|A\|_*$ . This is equal to the sum of all singular values of  $A$ , i.e.  $\|A\|_* = \text{tr}(\Sigma_r)$ , where  $\Sigma_r$  is defined in 2.6. The nuclear norm is also known as the **trace norm**, **Ky Fan  $r$ -norm**, or **Schatten 1-norm**.*

Any Stiefel manifold  $V_t(\mathbb{R}^s)$  has a left (resp. right) action of  $O(s)$  (resp.  $O(t)$ ) given by matrix multiplication.

**Proposition 2.5.** *The action of the orthogonal group  $O(t)$  (respectively,  $O(s)$ ) by right (respectively, left) matrix multiplication on  $V_t(\mathbb{R}^s)$  is an isometry with respect to  $D$ .*

*Proof.* Let  $A$  be an element of  $O(t)$ . The ambient inner product (2.2) is invariant with respect to the right action, as

$$(2.3) \quad \text{tr}((PA)^\top QA) = \text{tr}(A^\top P^\top QA) = \text{tr}(AA^\top P^\top Q) = \text{tr}(P^\top Q).$$

and similarly for the left action. ■

**2.3. Matrix decompositions.** Our method makes frequent use of the singular value and polar decomposition of matrices. For the sake of completeness, we have recorded the relevant details below.

**Definition 2.6 (Singular value decomposition (SVD)).** *For any matrix  $A \in \mathbb{R}^{s \times t}$ , there exists a set of matrices such that*

$$(2.4) \quad A = P \begin{bmatrix} \Sigma_r & 0 \\ 0 & 0_{s-r, t-r} \end{bmatrix} Q^\top$$

where  $r \leq \min\{s, t\}$  is the rank of  $A$ ,  $P \in \mathbb{R}^{s \times s}$ ,  $Q \in \mathbb{R}^{t \times t}$ ,  $P^\top P = I_s$ ,  $Q^\top Q = I_t$ , and  $\Sigma_r \in \mathbb{R}^{r \times r}$  is a diagonal matrix with nonnegative real numbers on the diagonal. The entries of  $\Sigma_r$  are known as **singular values** of  $A$ , and the columns of  $P$  and the columns of  $Q$  are the **left and right singular vectors** of  $A$ , respectively.

We note that while one matrix may have many forms of SVD, the set of singular values for a matrix  $A$  is unique. Related to the singular value decomposition of a matrix is its polar decomposition. The following is taken from [14].

**Theorem 2.7. (Polar decomposition)** *Let  $A \in \mathbb{R}^{s \times t}$  with  $s \geq t$ . There exists a matrix  $U \in \mathbb{R}^{s \times t}$  with orthonormal columns and a unique self-adjoint positive semidefinite matrix  $H \in \mathbb{R}^{t \times t}$  such that  $A = UH$ . The matrix  $H$  is given by  $H = (A^\top A)^{1/2}$ . All possible  $U$  are given by*

$$(2.5) \quad U = P \begin{bmatrix} I_r & 0 \\ 0 & W \end{bmatrix} Q^\top$$

where  $A = P \begin{bmatrix} \Sigma_r & 0 \\ 0 & 0_{s-r, t-r} \end{bmatrix} Q^\top$  is an SVD of  $A$  (2.6),  $r = \text{rank}(A)$ , and  $W \in \mathbb{R}^{(s-r) \times (t-r)}$  is arbitrary subject to having orthonormal columns. If  $\text{rank}(A) = t$ , then  $H$  is positive definite, hence invertible, and  $U$  is uniquely determined by  $U = AH^{-1}$ .

*Proof.* The analogous theorem over  $\mathbb{C}$  is proved in [14, Theorem 8.1, p. 193]. The non-trivial steps of the proof consist of finding a singular value decomposition of  $A$  and finding the unique square root of a positive semidefinite matrix. Both procedures are possible over  $\mathbb{R}$ . ■

## 2.4. Principal Component Analysis.

**Definition 2.8 (Principal Component Analysis (PCA)).** *Given data points  $y \in \mathcal{Y} \subset V_k(\mathbb{R}^N)$ , consider the sample covariance matrix  $\hat{\Sigma} = \frac{1}{|\mathcal{Y}|} \sum_{y \in \mathcal{Y}} yy^\top \in \mathbb{R}^{N \times N}$ . Apply eigendecomposition*

on  $\hat{\Sigma}$  to get  $N$  eigenvectors, each of which is an  $N$ -dimensional vector. Note that since  $\hat{\Sigma}$  is a real symmetric matrix, its eigenvalues are real and its eigenvectors can be selected to be orthonormal. Select  $n$  of the eigenvectors that correspond to the  $n$  highest eigenvalues of  $\hat{\Sigma}$ , and set them to be columns of  $\beta \in V_n(\mathbb{R}^N) \subset \mathbb{R}^{N \times n}$ . We refer to  $\beta$  as the output of PCA on  $\mathcal{Y}$ , or  $\text{PCA}(\mathcal{Y})$ .

## 2.5. Equivariance.

**Definition 2.9.** Let  $X, Y$  be spaces with an action of a group  $G$ , and  $f : X \rightarrow Y$  be a function. We say that  $f$  is  **$G$ -equivariant** if for all  $x \in X$  and  $g \in G$ , we have  $f(x \cdot g) = f(x) \cdot g$ . If furthermore  $G$  acts trivially on  $Y$ , then  $f$  is called  **$G$ -invariant**.

The definitions of  $G$ -equivariance and  $G$ -invariance also apply in the case of a function  $F : X \times X \rightarrow Y$  and a diagonal action of  $G$  on  $X \times X$ .

**3. Projection.** The purpose of this section is to define and prove several key properties of the projection  $\pi_\alpha$  referenced in Step 3 of Algorithm 1.1. The main result of this Section is Theorem 3.2, which uses the following Definition.

**Definition 3.1.** Let  $\alpha \in V_n(\mathbb{R}^N)$ . By slight abuse of notation, we let  $\alpha : V_k(\mathbb{R}^n) \rightarrow V_k(\mathbb{R}^N)$  be the map given by left matrix multiplication by  $\alpha$ .

Proposition 3.3 shows that this map is, in fact, an isometric embedding. We can now state the main result of this section.

**Theorem 3.2.** Fix an integer  $n$  and element  $\alpha \in V_n(\mathbb{R}^N)$  and consider the associated isometric embedding  $\alpha : V_k(\mathbb{R}^n) \rightarrow V_k(\mathbb{R}^N)$ . Let  $T \subset V_k(\mathbb{R}^N)$  be the set of points within  $\sqrt{2}$  of  $\text{im}(\alpha)$  with respect to the distance  $D$  (as in Definition 2.3). There is a continuous,  $O(k)$ -equivariant projection  $\pi_\alpha : T \rightarrow \alpha(V_k(\mathbb{R}^n)) = \text{im}(\alpha)$  such that for each fixed  $y \in T$ , the following holds:

$$(3.1) \quad D(y, \pi_\alpha(y)) \leq D(y, x) \text{ for all } x \in \alpha(V_k(\mathbb{R}^n)).$$

*Proof.* The projection  $\pi_\alpha$  is defined in Definition 3.4. That the domain of  $\pi_\alpha$  in Definition 3.4 coincides with  $T$  follows from Proposition 3.6. The equivariance of  $\pi_\alpha$  is Proposition 3.8. The claim in (3.1) follows from Propositions 3.9 and 3.10. Continuity of the projection is Theorem 3.7. ■

Before addressing the results referenced in the proof of Theorem 3.2, we include a proof of the following for the sake of completeness.

**Proposition 3.3.** For each  $\alpha \in V_n(\mathbb{R}^N)$ , the associated map from Definition 3.1 is an isometric embedding (with respect to  $D$ ) of  $V_k(\mathbb{R}^n)$  into  $V_k(\mathbb{R}^N)$ .

*Proof.* Let  $\alpha \in V_n(\mathbb{R}^N)$ , and consider any  $U, V \in V_k(\mathbb{R}^n)$ . Using the defining property in Proposition 2.2 and the invariance of trace under cyclic permutations, we see that:

$$\begin{aligned}
(3.2) \quad D^2(\alpha(U), \alpha(V)) &= \text{tr}((\alpha(U) - \alpha(V))(\alpha(U) - \alpha(V))^\top (\alpha(U) - \alpha(V))(\alpha(U) - \alpha(V))^\top) \\
(3.3) \quad &= \text{tr}(\alpha(U - V)(U - V)^\top \alpha^\top \alpha(U - V)(U - V)^\top) \\
(3.4) \quad &= \text{tr}(\alpha^\top \alpha(U - V)(U - V)^\top (U - V)(U - V)^\top) \\
(3.5) \quad &= D^2(U, V).
\end{aligned}$$

■

Figure 1.1 (left) shows a low-dimensional example of Proposition 3.3. Based on this observation, we propose the following approach. We seek an “optimal” embedding  $\alpha$  that describes our data, then use that  $\alpha$  to define an  $O(k)$ -equivariant projection  $\pi_\alpha : \mathcal{Y} \mapsto \alpha(\mathcal{Y}) \subset \alpha(V_k(\mathbb{R}^n))$ . Figure 1.1 (right) outlines our algorithm. We now define such a projection  $\pi_\alpha$  for any given  $\alpha$ . In Section 4, we discuss the problem of optimizing  $\alpha$  over  $V_n(\mathbb{R}^N)$  given the dataset.

**Definition 3.4.** (*Projection.*) Fix  $\alpha \in V_n(\mathbb{R}^N)$ . Let  $L = \{y \in V_k(\mathbb{R}^N) \mid \text{rank}(\alpha^\top y) < k\}$ . Define

$$\pi_\alpha : V_k(\mathbb{R}^N) \setminus L \rightarrow \alpha(V_k(\mathbb{R}^n))$$

as follows for an element  $y$  in the domain. Let  $\hat{y}_\alpha$  be the polar factor  $U$  in the polar decomposition of  $\alpha^\top y$ . Then  $\hat{y}_\alpha$  has orthonormal columns so  $\hat{y}_\alpha \in V_k(\mathbb{R}^n)$ . Define  $\pi_\alpha$  by  $\pi_\alpha(y) := \alpha \hat{y}_\alpha$ .

**Remark 3.5.** Note that on the set  $V_k(\mathbb{R}^N) \setminus L$ , we can define  $\pi_\alpha$  equivalently as follows. For  $y \in V_k(\mathbb{R}^N) \setminus L$ , let  $\alpha^\top y = P \begin{bmatrix} \Sigma_r & 0 \\ 0 & 0_{n-r, k-r} \end{bmatrix} Q^\top$  be any singular value decomposition of  $\alpha^\top y$ . Let  $\hat{y}_\alpha$  be given by

$$(3.6) \quad \hat{y}_\alpha = P \begin{bmatrix} I_k \\ 0 \end{bmatrix} Q^\top$$

and let  $\pi_\alpha(y) = \alpha(\hat{y}_\alpha)$ . For this to make sense, we must ensure that  $\hat{y}_\alpha$  is independent of the particular choice of singular value decomposition of  $\alpha^\top y$ . By Theorem 2.7,  $\hat{y}_\alpha$  is the polar factor in some polar decomposition of  $\alpha^\top y$ .

But since  $\alpha^\top y$  is assumed to have full rank, this factor is unique. In particular, if  $\alpha^\top y = P' \begin{bmatrix} \Sigma'_r & 0 \\ 0 & 0_{n-r, k-r} \end{bmatrix} Q'^\top$  is any other singular value decomposition of  $\alpha^\top y$ , we are guaranteed that

$$(3.7) \quad P \begin{bmatrix} I_k \\ 0 \end{bmatrix} Q^\top = P' \begin{bmatrix} I_k \\ 0 \end{bmatrix} Q'^\top$$

by the uniqueness in Theorem 2.7, so  $\hat{y}_\alpha$  is uniquely determined. It also follows from Theorem 2.7 that this  $\hat{y}_\alpha$  agrees with that in Definition 3.4.

The remainder of this section is devoted to proving that  $\pi_\alpha$  is well-defined on a suitable neighborhood in  $V_k(\mathbb{R}^N)$  (Proposition 3.6), that  $\pi_\alpha$  is continuous on this domain (Proposition 3.7), that  $\pi_\alpha$  is equivariant (Proposition 3.8) and that Equation (3.1) holds (Propositions 3.9 and 3.10).

**Proposition 3.6.** Given  $\alpha \in V_n(\mathbb{R}^N)$ ,  $x \in V_k(\mathbb{R}^n)$ ,  $y \in V_k(\mathbb{R}^N)$ , let  $\text{im}(\alpha)^\perp := \{y \in V_k(\mathbb{R}^N) \mid \langle y_i, \alpha_j \rangle = 0 \forall i, j\}$  so the columns  $y_i$  of  $y$  are pairwise orthogonal to the columns of  $\alpha$  as vectors in  $\mathbb{R}^N$ . We have that:

(a) If  $y \in \text{im}(\alpha)^\perp$  then  $\|y - \alpha x\|_F = \sqrt{2k}$ .

(b) If  $\|y - \alpha x\|_F < \sqrt{2}$  then  $\alpha^\top y$  is full rank, and so the map  $\pi_\alpha$  is well-defined.

Thus the map  $\pi_\alpha$  is well-defined on all points at distance less than  $\sqrt{2}$  from some element of  $\text{im}(\alpha)$ .

*Proof.* For (a), suppose that  $y \in \text{im}(\alpha)^\perp$ . Then, for  $x \in V_k(\mathbb{R}^n)$

$$\begin{aligned} D(y, \alpha x) &= \|y - \alpha x\|_F \\ &= \sqrt{\|y\|_F^2 - 2\langle y, \alpha x \rangle_D + \|\alpha x\|_F^2}. \end{aligned}$$

By assumption, the columns of  $y$  and  $\alpha x$  span orthogonal subspaces of  $\mathbb{R}^N$ . Hence, the inner product above is zero and the previous term, using 3.20, reduces to

$$\begin{aligned} &\sqrt{\|y\|_F^2 + \|\alpha x\|_F^2} \\ &= \sqrt{k + k} \\ &= \sqrt{2k} \end{aligned}$$

For (b) we prove the contrapositive: assuming that  $\alpha^\top y$  is not full rank we show that the distance is bounded below by  $\sqrt{2}$ . Let  $\alpha_i$  denote the  $i$ th column of  $\alpha$ , and let  $y_i$  denote the  $i$ th column of  $y$ . If  $\alpha^\top y$  does not have full rank, then there must be some dependence relation among the column vectors  $\{\alpha^\top y_1, \alpha^\top y_2, \dots, \alpha^\top y_k\}$ , meaning that  $\text{span}(\{y_i\})$  intersects  $\ker(\alpha^\top) = \text{span}(\{\alpha_i\})^\perp$  non-trivially, i.e.,  $\text{span}(\{y_i\}) \cap \text{span}(\{\alpha_i\})^\perp$  has nonzero dimension  $l > 0$ . Up to left multiplication by an element of  $O(k)$  we may assume the first  $l$  columns of  $y$  lie entirely in the orthogonal complement of  $\text{span}(\{\alpha_i\})$ .

In these coordinates, we may compute the distance between  $y$  and any element  $a \in \alpha(V_k(\mathbb{R}^n))$  as the sum of the squared norms of the columns of  $y - a$ . However, for  $1 \leq i \leq l$ , we know that  $y_i$  and  $a_i$  are unit vectors that are orthogonal to one another, and hence  $\|y_i - a_i\| = \sqrt{2}$ . Thus,  $D(y, a) = \|y - a\|_F \geq \sqrt{2}l \geq \sqrt{2}$ . ■

**Proposition 3.7.** Fix  $\alpha \in V_n(\mathbb{R}^N)$  and let

$$\pi_\alpha: V_k(\mathbb{R}^N) \setminus L \rightarrow \alpha(V_k(\mathbb{R}^n))$$

be as in Definition 3.4. On this (restricted) domain,  $\pi_\alpha$  is continuous.

*Proof.* Let  $y \in V_k(\mathbb{R}^N) \setminus L$  and let  $\alpha^\top y = UH$  be a polar decomposition (see Theorem 2.7) of  $\alpha^\top y$ . By definition,  $\pi_\alpha(y) = \alpha(\hat{y}_\alpha) = \alpha U$ . By assumption,  $\alpha^\top y$  has full rank, and so by Theorem 2.7, we have that  $U = \alpha^\top y H^{-1}$  and hence

$$(3.8) \quad \pi_\alpha(y) = \alpha \alpha^\top y H^{-1}$$

Denote by  $f$  the assignment of a matrix  $A$  to the positive semidefinite matrix  $H$  in the polar decomposition of  $A$ . It follows from, for instance, [14, Theorem 8.9] that  $f$  is continuous. Therefore,  $\pi_\alpha$  is given by

$$(3.9) \quad y \mapsto \alpha \alpha^\top y (f(\alpha^\top y))^{-1} \quad \blacksquare$$

which is a composition of continuous functions.

**Proposition 3.8.** *The map  $\pi_\alpha$  of Definition 3.4 is  $O(k)$ -equivariant. That is, for any  $g \in O(k)$ , we have  $\pi_\alpha(yg) = \pi_\alpha(y)g$ . Note that the group action is right matrix multiplication in both cases.*

*Proof.* Suppose  $y \in V_k(\mathbb{R}^N) \setminus L$  so that  $\alpha^\top y$  has full rank, i.e.,  $\text{rank}(\alpha^\top y) = k$ . Then let

$$(3.10) \quad \alpha^\top y = P \begin{bmatrix} \Sigma_r & 0 \\ 0 & 0_{n-r, k-r} \end{bmatrix} Q^\top$$

be any singular value decomposition of  $\alpha^\top y$ . Then  $\hat{y}_\alpha$  is given by

$$(3.11) \quad \hat{y}_\alpha = P \begin{bmatrix} I_k \\ 0 \end{bmatrix} Q^\top$$

and so

$$(3.12) \quad \pi_\alpha(y)g = \alpha P \begin{bmatrix} I_k \\ 0 \end{bmatrix} Q^\top g$$

Now let us compute  $\pi_\alpha(yg)$ . Note that since  $g$  has full rank, we are guaranteed that  $\alpha^\top yg$  does as well. Hence, as in Remark 3.5, we know that  $\widehat{yg}$  will be given by

$$(3.13) \quad \widehat{yg} = P' \begin{bmatrix} I_k \\ 0 \end{bmatrix} Q'^\top$$

where

$$(3.14) \quad \alpha^\top yg = P' \begin{bmatrix} \Sigma'_r & 0 \\ 0 & 0_{n-r, k-r} \end{bmatrix} Q'^\top$$

is any singular value decomposition of  $\alpha^\top yg$ . In particular, note that

$$(3.15) \quad \alpha^\top yg = P \begin{bmatrix} \Sigma_r & 0 \\ 0 & 0_{n-r, k-r} \end{bmatrix} (g^\top Q)^\top$$

is a singular value decomposition of  $\alpha^\top yg$ . Hence,  $\widehat{yg}$  will be given by

$$(3.16) \quad \widehat{yg} = P \begin{bmatrix} I_k \\ 0 \end{bmatrix} (g^\top Q)^\top$$

and so  $\pi_\alpha(yg)$  will be given by

$$(3.17) \quad \alpha P \begin{bmatrix} I_k \\ 0 \end{bmatrix} (g^\top Q)^\top = \alpha P \begin{bmatrix} I_k \\ 0 \end{bmatrix} Q^\top g$$

Comparing (3.12) and (3.17) completes the proof. \blacksquare

The following two propositions together show that our projection minimizes the distance each  $y$  travels to  $\pi_\alpha(y)$  for a fixed  $\alpha$ , and thus minimizes “distortion” of the data.

**Proposition 3.9.** *For a fixed  $\alpha \in V_n(\mathbb{R}^N)$ , let  $y \in V_k(\mathbb{R}^N)$ . As defined above,  $\hat{y}_\alpha \in V_k(\mathbb{R}^n)$  achieves the minimum distance  $D$  between  $\alpha^\top y \in \mathbb{R}^{n \times k}$  and points in  $V_k(\mathbb{R}^n)$ .*

*Proof.* It is shown in [14, 8.4], where it is attributed to [10], that

$$(3.18) \quad \hat{y}_\alpha = \operatorname{argmin}_{Q \in \mathbb{C}^{n \times k}} \left\{ \|\alpha^\top y - Q\| \mid Q^*Q = I_k \right\}$$

for any unitarily invariant norm. Since

$$(3.19) \quad \min_{Q \in \mathbb{C}^{n \times k}} \left\{ \|\alpha^\top y - Q\| \mid Q^*Q = I_k \right\} \leq \min_{Q \in \mathbb{R}^{n \times k}} \left\{ \|\alpha^\top y - Q\| \mid Q^*Q = I_k \right\}$$

and  $\hat{y}_\alpha$  in fact has real entries, the fact that  $D$  is unitarily invariant when viewed as a norm on  $\mathbb{C}^{n \times k}$  completes the argument.

A direct proof for  $D(P, Q) = \|P - Q\|_F$  can be found in [17]. ■

**Proposition 3.10.** *Fix the distance  $D$ ,  $\alpha \in V_n(\mathbb{R}^N)$ , and  $y \in V_k(\mathbb{R}^N)$ . Let  $x \in V_k(\mathbb{R}^n)$  be a (not necessarily unique) point of minimal distance on  $V_k(\mathbb{R}^n)$  to  $\alpha^\top y \in \mathbb{R}^{n \times k}$ . Then a (not necessarily unique) point of minimal distance on  $\alpha(V_k(\mathbb{R}^n))$  to  $y$  is  $\alpha(x)$ .*

*Proof.* First, note that for any  $x \in V_t(\mathbb{R}^s)$ ,  $t < s$ , we have

$$(3.20) \quad \|x\|_F^2 = \operatorname{tr}(x^\top x) = \operatorname{tr}(I_t) = t,$$

$$(3.21) \quad \|xx^\top\|_F^2 = \operatorname{tr}(xx^\top xx^\top) = \operatorname{tr}(xx^\top) = t.$$

We have  $\|y - \alpha u\|_D = \sqrt{2k - 2\langle y, \alpha u \rangle_D} = \sqrt{2k - 2\langle \alpha^\top y, u \rangle_D}$ , so  $u$  that minimizes  $\|y - \alpha u\|_D =$  maximizes  $\langle \alpha^\top y, u \rangle_D =$  minimizes  $\|\alpha^\top y - u\|_D$ .

Furthermore:

$$\begin{aligned} & \arg \min_{u \in V_k(\mathbb{R}^n)} \|y - \alpha u\|_F \\ &= \arg \min_{u \in V_k(\mathbb{R}^n)} \sqrt{\|y\|_F^2 - 2\langle y, \alpha u \rangle_D + \|\alpha u\|_F^2} \\ &= \arg \min_{u \in V_k(\mathbb{R}^n)} \sqrt{2k - 2\langle y, \alpha u \rangle_D} \\ &= \arg \max_{u \in V_k(\mathbb{R}^n)} \langle y, \alpha u \rangle_D \\ &= \arg \max_{u \in V_k(\mathbb{R}^n)} \langle \alpha^\top y, u \rangle_D \\ &= \arg \min_{u \in V_k(\mathbb{R}^n)} -2\langle \alpha^\top y, u \rangle_D \\ &= \arg \min_{u \in V_k(\mathbb{R}^n)} \|\alpha^\top y\|_F^2 - 2\langle \alpha^\top y, u \rangle_D + k \\ &= \arg \min_{u \in V_k(\mathbb{R}^n)} \sqrt{\|\alpha^\top y\|_F^2 - 2\langle \alpha^\top y, u \rangle_D + \|u\|_F^2} \\ &= \arg \min_{u \in V_k(\mathbb{R}^n)} \|\alpha^\top y - u\|_F \end{aligned}$$

We can add  $\|\alpha^\top y\|_{\mathbb{F}}^2$  without a problem because the function only depends on  $u$ , i.e.  $\alpha^\top y$  is fixed. ■

**4. Optimization.** In this section, we discuss our process for optimizing  $\alpha$  over  $V_n(\mathbb{R}^N)$ , detailing Steps 4 and 5 of Algorithm 1.1. A projection  $\alpha \in V_n(\mathbb{R}^N)$  is considered to be optimal if it minimizes the cost function, defined as the sum over data points  $y_i \in Y$  of the squared distance between  $y_i$  and its image under the map  $\pi_\alpha$ . We approximate a solution to this minimization problem using the software package Pymanopt [34].

The package Pymanopt implements algorithms for manifold optimization that are intrinsic to the manifold. Inputs include a manifold, which in our case is  $V_n(\mathbb{R}^N)$ , a cost function, and sometimes derivatives of the cost function.

We now show how we manipulate our cost function into a function with the same optimizer that we are able to input into Pymanopt.

**Proposition 4.1.** *The optimization problem*

$$(4.1) \quad \arg \min_{\alpha \in V_n(\mathbb{R}^N)} \frac{1}{|\mathcal{Y}|} \sum_{y \in \mathcal{Y}} \|y - \pi_\alpha(y)\|^2$$

is equivalent to (i.e. has the same solution as)

$$(4.2) \quad \arg \max_{\alpha \in V_n(\mathbb{R}^N)} \frac{1}{|\mathcal{Y}|} \sum_{y \in \mathcal{Y}} \|\alpha^\top y\|_*.$$

*Proof.* An optimal value of  $\alpha$ , denoted  $\hat{\alpha}$ , is one that minimizes the mean of the sum of squares of distances from data points  $y$  to their projections  $\pi_\alpha(y)$ . That is,

$$(4.3) \quad \hat{\alpha} = \arg \min_{\alpha \in V_n(\mathbb{R}^N)} \frac{1}{|\mathcal{Y}|} \sum_{y \in \mathcal{Y}} \|y - \pi_\alpha(y)\|^2.$$

By Definition 3.4, we have  $\pi_\alpha(y) = \alpha(\hat{y}_\alpha)$ , where  $\hat{y}_\alpha$  is the polar factor in a polar decomposition of  $\alpha^\top y$ . So

$$(4.4) \quad \hat{\alpha} = \arg \min_{\alpha \in V_n(\mathbb{R}^N)} \frac{1}{|\mathcal{Y}|} \sum_{y \in \mathcal{Y}} \|y - \alpha(\hat{y}_\alpha)\|^2.$$

Rearranging terms in this product of vectors gives

$$(4.5) \quad \hat{\alpha} = \arg \min_{\alpha \in V_n(\mathbb{R}^N)} \frac{1}{|\mathcal{Y}|} \sum_{y \in \mathcal{Y}} (\|y\|^2 - 2\langle y, \alpha(\hat{y}_\alpha) \rangle + \|\alpha(\hat{y}_\alpha)\|^2).$$

Since the set  $Y$  is constant across all  $\alpha$ , the term  $\|y\|^2$  does not affect the minimizer. Thus

$$(4.6) \quad \hat{\alpha} = \arg \min_{\alpha \in V_n(\mathbb{R}^N)} \frac{1}{|\mathcal{Y}|} \sum_{y \in \mathcal{Y}} (-2\langle y, \alpha(\hat{y}_\alpha) \rangle + \|\alpha(\hat{y}_\alpha)\|^2).$$

Note that for all  $y$ , we have  $\alpha(\hat{y}_\alpha) \in V_k(\mathbb{R}^N)$ . Thus  $\|\alpha(\hat{y}_\alpha)\|^2 = k$ , a constant term which does not affect the optimizer, so we have

$$(4.7) \quad \hat{\alpha} = \arg \min_{\alpha \in V_n(\mathbb{R}^N)} \frac{1}{|\mathcal{Y}|} \sum_{y \in \mathcal{Y}} -2\langle y, \alpha(\hat{y}_\alpha) \rangle.$$

Negating changes a minimizer to a maximizer, and scaling by a positive constant does not affect the maximizer, so we have

$$(4.8) \quad \hat{\alpha} = \arg \max_{\alpha \in V_n(\mathbb{R}^N)} \frac{1}{|\mathcal{Y}|} \sum_{y \in \mathcal{Y}} \langle y, \alpha(\hat{y}_\alpha) \rangle.$$

For any matrix  $A$  and its conjugate transpose  $A^*$ , and vectors  $v, w$ , the following property holds for the inner product associated to  $D$ :  $\langle Av, w \rangle = \langle v, A^*w \rangle$ .

Since  $\alpha$  has real entries, its conjugate transpose is its transpose  $\alpha^\top$ . Since  $\alpha$  is orthonormal,  $\alpha^\top \alpha$  is the identity matrix. So we have

$$(4.9) \quad \hat{\alpha} = \arg \max_{\alpha \in V_n(\mathbb{R}^N)} \frac{1}{|\mathcal{Y}|} \sum_{y \in \mathcal{Y}} \langle \alpha^\top y, \hat{y} \rangle.$$

By Definition 3.4, we have

$$(4.10) \quad \hat{\alpha} = \arg \max_{\alpha \in V_n(\mathbb{R}^N)} \frac{1}{|\mathcal{Y}|} \sum_{y \in \mathcal{Y}} \left\langle P_y \begin{bmatrix} \Sigma_y & 0 \\ 0 & 0_{n-r_y, k-r_y} \end{bmatrix} (g^\top Q_y)^\top, P_y \begin{bmatrix} I_{r_y} & 0 \\ 0 & 0_{n-r_y, k-r_y} \end{bmatrix} (g^\top Q_y)^\top \right\rangle.$$

The following depends on a choice of norm. For  $D$ , we continue as follows. We start with

$$(4.11) \quad \hat{\alpha} = \arg \max_{\alpha \in V_n(\mathbb{R}^N)} \frac{1}{|\mathcal{Y}|} \sum_{y \in \mathcal{Y}} \text{tr} \left( g^\top Q_y \begin{bmatrix} \Sigma_y & 0 \\ 0 & 0_{k-r_y, n-r_y} \end{bmatrix} P_y^\top P_y \begin{bmatrix} I_{r_y} & 0 \\ 0 & 0_{n-r_y, k-r_y} \end{bmatrix} Q_y^\top g \right).$$

Using the fact that  $g, Q_y$ , and  $P_y$  are orthogonal, and using the fact that the trace is invariant under cycle permutations, we obtain:

$$(4.12) \quad \hat{\alpha} = \arg \max_{\alpha \in V_n(\mathbb{R}^N)} \frac{1}{|\mathcal{Y}|} \sum_{y \in \mathcal{Y}} \text{tr} \left( \begin{bmatrix} \Sigma_y & 0 \\ 0 & 0_{k-r_y, k-r_y} \end{bmatrix} \right).$$

Using the nuclear norm as defined in Definition 2.4, we have

$$(4.13) \quad \hat{\alpha} = \arg \max_{\alpha \in V_n(\mathbb{R}^N)} \frac{1}{|\mathcal{Y}|} \sum_{y \in \mathcal{Y}} \|\alpha^\top y\|_*.$$

The nuclear norm is non-differentiable, but it does have a subgradient, which is used as the “gradient” for many gradient-based (i.e. first-order) optimization methods. ■

*Remark 4.2.* Another reasonable choice for the loss function would be

$$(4.14) \quad \min_{\alpha \in V_n(\mathbb{R}^N)} \frac{1}{|\mathcal{Y}|} \sum_{y \in \mathcal{Y}} \|y - \pi_\alpha(y)\| = \min_{\alpha \in V_n(\mathbb{R}^N)} \frac{1}{|\mathcal{Y}|} \sum_{y \in \mathcal{Y}} \sqrt{2k - 2\|\alpha^\top y\|_*},$$

which comes from the proof of Proposition 4.1. This problem can then be optimized using gradient descent, and Lemma 4.4 holds true for (4.14) as well. This is because the Euclidean gradient of (4.14) is just a scaled version of the Euclidean gradient of (4.2) with the same subspace. For all  $y \in \mathcal{Y}$ , using chain rule:

$$\begin{aligned} \frac{\partial}{\partial \alpha} \sqrt{2k - 2\|\alpha^\top y\|_*} &= \frac{1}{2} (2k - 2\|\alpha^\top y\|_*)^{-\frac{1}{2}} \frac{\partial}{\partial \alpha} (2k - 2\|\alpha^\top y\|_*) \\ &= - (2k - 2\|\alpha^\top y\|_*)^{-\frac{1}{2}} y \hat{y}_\alpha^\top. \end{aligned}$$

**4.1. PCA is a critical point when data comes from a low-dimensional manifold.** We now show that if the considered data  $\mathcal{Y} \subset V_k(\mathbb{R}^N)$  lies precisely in the image  $\alpha(V_k(\mathbb{R}^n))$  of an embedded lower-dimensional Stiefel manifold, then the  $\alpha$  obtained from PCA (see Definition 2.8) is a critical point of the optimization problem defined in (4.2). That is, we temporarily work under the following.

**Assumption 4.3.** For a fixed  $\alpha \in V_n(\mathbb{R}^N)$ , for all  $y \in \mathcal{Y} \subset V_k(\mathbb{R}^N)$ , there exists an  $x \in \mathcal{X} \subset V_k(\mathbb{R}^n)$  such that  $y = \alpha(x)$ .

Assumption 4.3 means our data really does come from a lower-dimensional space. Another informal interpretation could be that there is no high-dimensional noise, so the columns of the  $y$  span a proper subspace of  $\mathbb{R}^N$  with dimension  $n$ .

**Lemma 4.4.** Under Assumption 4.3,  $\beta$  (2.8) is a critical point of the optimization problem defined in (4.2).

*Proof.* We evaluate the gradient directly. The Euclidean gradient of (4.2) at any  $\alpha \in V_n(\mathbb{R}^N)$  is

$$(4.15) \quad \frac{\partial}{\partial \alpha} f(\alpha) = \frac{\partial}{\partial \alpha} \frac{1}{|\mathcal{Y}|} \sum_{y \in \mathcal{Y}} \|\alpha^\top y\|_* = \frac{1}{|\mathcal{Y}|} \sum_{y \in \mathcal{Y}} \frac{\partial}{\partial \alpha} \|\alpha^\top y\|_* = \frac{1}{|\mathcal{Y}|} \sum_{y \in \mathcal{Y}} y \hat{y}_\alpha^\top.$$

We project that gradient on to  $V_n(\mathbb{R}^N)$ , obtaining

$$(4.16) \quad \frac{1}{2} \alpha \left( \alpha^\top \frac{\partial}{\partial \alpha} f(\alpha) - \left( \alpha^\top \frac{\partial}{\partial \alpha} f(\alpha) \right)^\top \right) + (I_N - \alpha \alpha^\top) \frac{\partial}{\partial \alpha} f(\alpha)$$

$$(4.17) \quad = \frac{1}{|\mathcal{Y}|} \sum_{y \in \mathcal{Y}} (I_N - \alpha \alpha^\top) y \hat{y}_\alpha^\top = (I_N - \alpha \alpha^\top) \frac{1}{|\mathcal{Y}|} \sum_{y \in \mathcal{Y}} y \hat{y}_\alpha^\top,$$

where the first term of (4.16) is 0 since the following matrix is symmetric:

$$(4.18) \quad \alpha^\top \frac{\partial}{\partial \alpha} f(\alpha) = (\alpha^\top y) \hat{y}_\alpha^\top = (P \Sigma Q^\top) (P Q^\top)^\top = P \Sigma P^\top.$$

The columns of  $y\hat{y}_\alpha$  are linear combinations of the columns of  $y$ . Left multiplication by  $I_N - \alpha\alpha^\top$  projects those columns to the subspace that is orthogonal to the column space of  $\alpha$ . Because  $y$  is in the column space of  $\beta$  for all  $y \in \mathcal{Y}$  under Assumption 4.3, the Riemannian gradient is zero when evaluated at  $\alpha = \beta$ . ■

**Theorem 4.5.** *Under Assumption 4.3,  $\beta$  (2.8) is a global maximum of (4.2).*

*Proof.* The cost function evaluated at arbitrary  $\alpha \in V_n(\mathbb{R}^N)$  is a sum of terms of the form  $\|\alpha^\top(y)\|_*$  where  $\|\cdot\|_*$  denotes the nuclear norm, the sum of singular values. Moreover, by assumption the  $y$  come from a lower-dimensional space, so

$$\frac{1}{|\mathcal{Y}|} \sum_{y \in \mathcal{Y}} \|\alpha^\top(y)\|_* = \frac{1}{|\mathcal{X}|} \sum_{x \in \mathcal{X}} \|\alpha^\top(A(x))\|_*.$$

Note that the nuclear norm of the  $n \times k$  matrix  $\alpha^\top A(x)$  is bounded above by  $k$  times the operator norm, since the operator norm is the largest singular value. Moreover, the operator norm is submultiplicative, so

$$\begin{aligned} & \frac{1}{|\mathcal{X}|} \sum_{x \in \mathcal{X}} \|\alpha^\top(A(x))\|_* \\ & \leq \frac{1}{|\mathcal{X}|} \sum_{x \in \mathcal{X}} k \cdot \|\alpha^\top(A(x))\|_{op} \\ & \leq \frac{1}{|\mathcal{X}|} \sum_{x \in \mathcal{X}} k \cdot \|\alpha^\top\|_{op} \|A\|_{op} \|x\|_{op}. \end{aligned}$$

But each of  $\alpha^\top, A, y$  are elements of Stiefel manifolds and so their singular values are all 1. So the cost function is bounded above by  $k$ , and since the case  $\alpha = A$  realizes this upper bound, it is the global maximum.

For any output  $\alpha$  of PCA on  $\mathcal{Y}$  under these assumptions, we must have  $A = \alpha g$  for  $g \in O(n)$ , since they span the same column space. In which case

$$\|A^\top(y)\|_* = \|(\alpha g)^\top y\|_* = \|g^\top \alpha^\top y\|_* = \|\alpha^\top y\|_*$$

where the last line holds because any SVD decomposition  $U\Sigma V$  for  $\alpha^\top y$  induces one for  $g^\top \alpha^\top y$  by  $g^\top U\Sigma V$ , so they have the same singular values. So any output of PCA is a maximum for the cost function. ■

The following is a corollary of Lemma 4.4 and the last paragraph of the previous proof.

**Corollary 4.6.** *Let  $\beta' \in V_n(\mathbb{R}^N) \subset \mathbb{R}^{N \times n}$  be any point on the Stiefel manifold such that its columns span the same subspace as  $\beta$  (2.8). In other words,  $\beta'$  and  $\beta$  map to the same point on the Grassmannian, and  $\beta' = \beta g$  for some  $g \in O(k)$ . Then under Assumption 4.3,  $\beta'$  is also a critical point and a global maximizer of the optimization problem (4.2). This directly follows from the proof of Lemma 4.4 and Theorem 4.5.*

Lemma 4.4 and Theorem 4.5 together show that  $\alpha_{PCA}$  is a critical point and a global optimizer of (4.2) under Assumption 4.3. This is a nontrivial result given that the optimization problem over  $V_n(\mathbb{R}^N)$  is not convex. Therefore, we choose  $\alpha_{PCA}$  as the initialization point for the gradient descent step in PSC, with the understanding that if the data happens to come from exactly  $V_k(\mathbb{R}^n)$ , the gradient descent output  $\alpha_{GD}$  will be identical to  $\alpha_{PCA}$ . However, it is important to note that Assumption 4.3 is quite stringent and unlikely to hold in most real-world settings due to noise and variability in data. In those cases, the theoretical guarantee for  $\alpha_{PCA}$  no longer holds, and  $\pi_{\alpha_{GD}}$  will lead to a smaller projection error compared to  $\pi_{\alpha_{PCA}}$ . Section 5 empirically shows that this is indeed the case.

To summarize, the following always holds due to properties of gradient descent when initialized with  $\alpha_{PCA}$ :

$$(4.19) \quad \frac{1}{|\mathcal{Y}|} \sum_{y \in \mathcal{Y}} \|y - \pi_{\alpha_{GD}}(y)\|^2 \leq \frac{1}{|\mathcal{Y}|} \sum_{y \in \mathcal{Y}} \|y - \pi_{\alpha_{PCA}}(y)\|^2,$$

and equality is achieved if Assumption 4.3 is true.

We conclude this section with the following remark on equivariance versus invariance.

*Remark 4.7 (PCA is  $O(k)$ -invariant).* PCA in Definition 2.8 is  $O(k)$ -invariant, not  $O(k)$ -equivariant. In other words, for some  $g \in O(k)$ , the output of PCA on data points  $y \in \mathcal{Y}$  is identical to that of PCA on  $\{yg \mid y \in \mathcal{Y}\}$ . This follows from noticing that

$$(4.20) \quad \hat{\Sigma} = \frac{1}{|\mathcal{Y}|} \sum_{y \in \mathcal{Y}} (yg)(yg)^\top = \frac{1}{|\mathcal{Y}|} \sum_{y \in \mathcal{Y}} y(gg^\top)y^\top = \frac{1}{|\mathcal{Y}|} \sum_{y \in \mathcal{Y}} yy^\top.$$

However, if we use PCA as a way to choose an  $\alpha$  to use in  $\pi_\alpha$  in Definition 3.4, then our entire projection algorithm (which includes both finding  $\alpha$  from  $y$  and applying  $\pi_\alpha$  to  $y$ ) is  $O(k)$ -equivariant. That is,

$$(4.21) \quad \pi_{\text{PCA}(yg)}(yg) = \pi_{\text{PCA}(y)}(yg) = \pi_{\text{PCA}(y)}(y)g.$$

The last equality follows from Proposition 3.8, which shows that  $\pi_\alpha$  is equivariant for any fixed  $\alpha$ .

**4.2. Computational complexity of PSC.** Now that all elements of Algorithm 1.1 have been introduced, we analyze the runtime complexity of PSC. First, obtaining  $\alpha_{PCA}$  requires the following computationally costly steps:

- Constructing the covariance matrix  $\hat{\Sigma}$  from  $\mathcal{Y}$ . Naive multiplication of  $N \times k$  and  $k \times N$  matrices cost  $O(kN^2)$ , so the total cost would be  $O(|\mathcal{Y}|kN^2)$ .
- Performing eigenvalue decomposition (EVD) on  $\hat{\Sigma}$ . A full EVD costs  $O(N^3)$ , but iterative methods such as the power method or the Lanczos algorithm can calculate the top  $k$  eigenvectors of a positive semi-definite matrix in a reduced runtime of  $O(kN^2)$ . See [13, Section 8, 9] for a more thorough analysis. Note that we do not expect  $\hat{\Sigma}$  to be sparse.

In computing  $\hat{y}_\alpha$  for a given  $y$  and  $\alpha$ , we need to consider two costs:

- Naively multiplying  $\alpha^\top$  to all  $y \in \mathcal{Y}$  takes  $O(|\mathcal{Y}|Nnk)$ .

- Computing polar decomposition of  $\alpha^\top y$  for all  $y \in \mathcal{Y}$  can be done using singular value decomposition (SVD) in  $O(|\mathcal{Y}|k^2N)$ .

Next, performing gradient descent on  $V_n(\mathbb{R}^N)$  to find  $\alpha_{GD}$  relies heavily on the gradient calculation, which is done explicitly in the proof of Lemma 4.4.

- Calculation of  $I_N - \alpha\alpha^\top$  only needs to be done once for all  $\mathcal{Y}$  in  $O(nN^2)$ .
- As established earlier,  $\hat{y}_\alpha$  for all  $y \in \mathcal{Y}$  takes  $O(|\mathcal{Y}|Nnk)$ . So does matrix multiplication and addition for  $\sum_{y \in \mathcal{Y}} y\hat{y}_\alpha^\top$ .

Putting it together, computing (4.17) costs  $O(nN^2 + |\mathcal{Y}|Nnk)$  per gradient descent iteration. We noticed in our experiments that because we are warm-starting from  $\alpha_{PCA}$ , gradient descent terminates fairly quickly in practice.

Lastly,  $\pi_\alpha$  involves multiplying  $\alpha_{GD}$  to all  $\hat{y}_{\alpha_{GD}}$ , which is an  $O(|\mathcal{Y}|Nnk)$  operation.

We conclude that the computational complexity of PSC is  $O(|\mathcal{Y}|kN^2 + t(nN^2 + |\mathcal{Y}|Nnk))$ , where  $t$  is the number of gradient descent iterations. If  $|\mathcal{Y}| \gg N/k$  and  $N \gg n > k$ , this is simplified to  $O(|\mathcal{Y}|N^2 + t|\mathcal{Y}|N)$ . Speedup may be achieved by distributing computing across  $\mathcal{Y}$ , but we leave faster implementation of PSC to future work.

**5. Numerical Experiments.** In this section, we conduct several experiments on synthetic and real-world data to showcase the efficacy of our approach. Our Python code is freely available at <https://www.github.com/HarlinLee/PSC>.

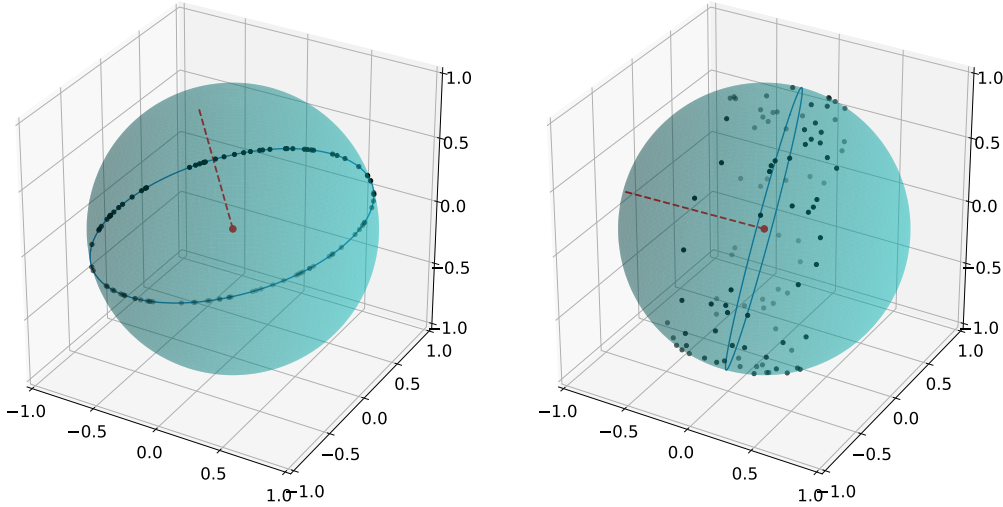


**Figure 5.1.** 100 data samples  $\mathcal{Y} \subset V_1(\mathbb{R}^3)$  generated with noise level  $\varepsilon = 0$  (left) and  $\varepsilon = 0.5$  (right). Without noise, all samples lie on the great circle, whose orientation and embedding in the sphere are determined by  $\alpha$  as shown in Figure 1.1.

**5.1. Low-dimensional visualization.** We start by illustrating our algorithm using a low-dimensional example where  $N = 3, n = 2, k = 1$ . First, we collect 100 noisy data samples  $\mathcal{Y} \subset V_k(\mathbb{R}^N)$  in the following manner. One hundred points  $\mathcal{X} \subset V_k(\mathbb{R}^n)$  are selected from the uniform distribution on  $V_k(\mathbb{R}^n)$  [5], then mapped to  $V_k(\mathbb{R}^N)$  using an  $\alpha \in V_n(\mathbb{R}^N)$  again from the uniform distribution. In this setting,  $\alpha$  embeds the unit circle  $S^1 \subset \mathbb{R}^2$  as a great circle

in the unit sphere  $S^2 \subset \mathbb{R}^3$ .

If desired, we may perturb each point  $x_i$  slightly by some distance  $\varepsilon > 0$  in the following way. For each  $x_i$  we randomly sample a unit vector  $u_i \in \varepsilon \cdot S^{N-1} \subset \mathbb{R}^N$ , add this to  $x_i$ , and project this perturbed vector back on to  $V_k(\mathbb{R}^N)$ . The resulting points lie in a neighborhood of the image of  $\alpha$ . See Figure 5.1 for examples. We set  $\varepsilon = 0.8$  in the following experiment.

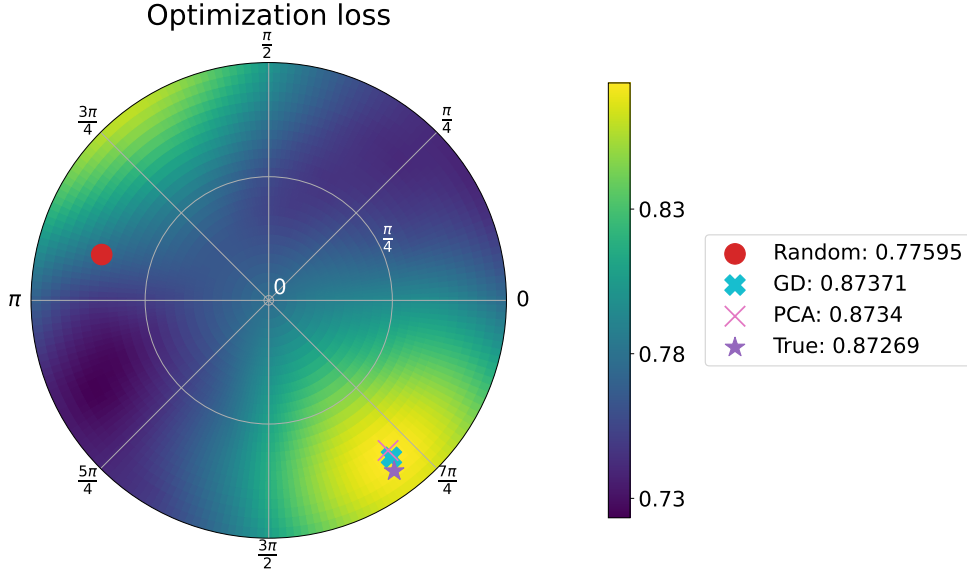


**Figure 5.2.** Optimization loss landscape (4.2) over the projections of  $\alpha \in V_2(\mathbb{R}^3)$  to the Grassmannian  $Gr(1, 3) = \mathbb{R}P^2$ . Input data are 100 noisy samples  $\mathcal{Y}$  with  $\varepsilon = 0.8$ . As described below, the loss function (4.2) descends to  $Gr(1, 3)$  which we plot as the upper hemisphere of  $S^2$ . The azimuthal angle is  $\theta \in [0, 2\pi]$  and the inclination angle is  $\phi \in [0, \frac{\pi}{2}]$  in this polar coordinate plot. Higher function values correspond to lower projection error. “True” is the  $\alpha$  used to generate the noisy samples. GD is the output of PSC after gradient descent.

Figure 5.2 plots the optimization loss landscape (4.2) as a function of  $\alpha \in V_n(\mathbb{R}^N)$ , or more specifically, as a function of the line normal to the column space of  $\alpha$ . These lines are the span of the red dashed vectors in Figures 1.1 and 5.1. They uniquely define the great circle used to generate the data, and therefore also define  $\alpha$  up to an element of  $O(2)$ . In practice, we calculated these normal vectors simply by taking the cross product of the columns of  $\alpha$ , and multiplying it by  $-1$  if needed to obtain its representative in our model of  $\mathbb{R}P^2$ . The normal vectors are transformed from Cartesian coordinates  $(x, y, z)$  to spherical coordinates using the formula azimuthal angle  $\theta = \tan^{-1}(y/x)$  and polar or inclination angle  $\phi = \cos^{-1}(z/\sqrt{x^2 + y^2 + z^2})$ .

The yellow region in Figure 5.2 shows the maximum of the loss function here. Note that this region overlaps with the boundary, and continues on the antipodal side of the disc as expected. In this highly noisy setting,  $\alpha_{PCA}$  or  $\alpha_{GD}$  achieve better performance (i.e. lower projection error) than the actual  $\alpha$  (True) that was used in data generation. Lastly, there is a difference between  $\alpha_{PCA}$  and  $\alpha_{GD}$ , showing that the gradient descent algorithm works as it should and is meaningful when the data does not entirely come from a low-dimensional space

(e.g.  $\varepsilon > 0$ ).

**5.2. Simulation experiment.** In this section, we compare our algorithm to principal geodesic analysis (PGA) as described in [12]. The package Geomstats [22] was used to apply PGA to data generated synthetically using the process of the previous section. To evaluate the performance of our method, we compare the ratios of appropriately defined variance when projecting using PGA as opposed to PSC. To define this variance we first define the intrinsic Frechet mean, i.e. a minimizer of the following function computed with gradient descent. Distance here is measured with respect to the Riemannian metric induced by the embedding of  $V_k(\mathbb{R}^N)$  in  $\mathbb{R}^{N \times k}$ .

$$\mu_{FM}(\mathcal{Y}) = \operatorname{argmin}_{\mu \in V_k(\mathbb{R}^N)} \sum_{y \in \mathcal{Y}} d(\mu, y)^2.$$

It is possible that a mean defined in this way is not unique, especially in the case where the points  $S$  lie on a lower-dimensional submanifold with some symmetry.

Letting  $\mu_{FM}$  denote the mean as above, we then define the Frechet variance as

$$\sigma^2(\mathcal{Y}) = \frac{1}{|\mathcal{Y}|} \sum_{y \in \mathcal{Y}} d(y - \mu_{FM})^2.$$

Here we set  $s = 200, N = 11, n = 6, k = 1, \varepsilon \in \{0.01, 0.05, 0.1, 0.5\}$ , and then apply the procedure described above to generate synthetic data. We then apply both our algorithm and PGA to reduce the dimension, and compute the variance of the projected data.

The variance ratio is the quotient of the two variances mentioned above. Each ratio for a fixed dimension of submanifold (either Stiefel in the case of PSC or geodesic in the case of PGA) is shown on the vertical axis of Figure 5.3. Each experiment was performed 100 times, and the results shown in the figure are averaged over 100 iterations.

From this standpoint of expressed variance, our algorithm outperforms PGA for smaller numbers of principal components, capturing a larger amount of the variance contained in the data. Moreover, PSC’s advantage over PGA increases as  $\varepsilon$  increases, demonstrating a robustness to higher levels of noise.

**5.3. Application to brain connectivity matrices.** Next, we show how our algorithm can be applied to real-world data. In many neuroscience applications, brains are divided into  $N$  regions before their activities are measured by, for example, fMRI. Positive semidefinite (PSD) matrices in  $\mathbb{R}^{N \times N}$  naturally arise in this context as graph adjacency matrices, graph Laplacian matrices, network connectivity matrices, and partial correlation matrices [21, 23, 32]. As eigenvectors contain important information about these matrices [1], it is intuitive to represent the set of top  $k$  eigenvectors as an orthonormal  $k$ -frame and thus as a point in the Stiefel manifold  $V_k(\mathbb{R}^N)$ . They can then be used for various downstream tasks such as clustering and brain-computer-interface control, for which dimensionality reduction is useful.

In this section, we demonstrate our algorithm on pairwise functional connectivity matrices between  $N = 83$  brain regions, using data from [23]. This is derived from three scans from eight subjects, resulting in a dataset  $Y$  of 24 PSD matrices in  $\mathbb{R}^{83 \times 83}$ . From each matrix, we took  $k = 1$  eigenvector corresponding to the largest eigenvalue as in [21], and for each of

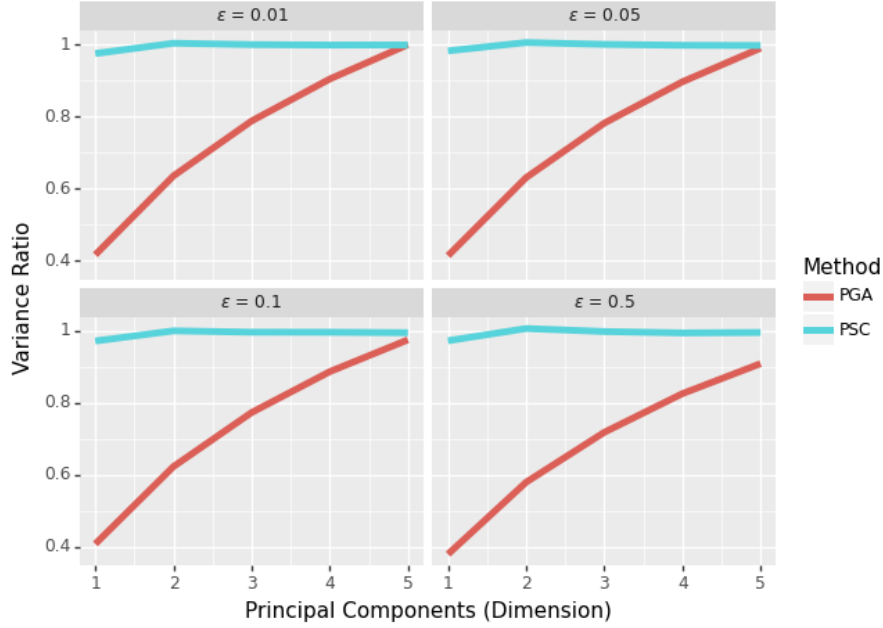


**Figure 5.3.** Variance ratio for PSC compared to principal geodesic analysis.

the resulting 24 data points on  $V_1(\mathbb{R}^{83})$ , we projected them to  $V_1(\mathbb{R}^3)$ , i.e.  $n = 3$ , using our proposed algorithm.

On the left side of Figure 5.4, we plot the 24 data points projected onto  $V_1(\mathbb{R}^3)$ . They are colored according to the eight human subjects. The right plot in Figure 5.4 shows the zoomed-in and birds-eye view of the data after all points in the lower hemisphere are reflected across the  $z = 0$  plane to the upper hemisphere. Samples from the same human subjects seem to sit closer to each other, which is remarkable given the amount of information that was lost when dimensionality was reduced from 3,  $403 = (83^2 - 83)/2$  unique numbers in  $\mathbb{R}^{83 \times 83}$  to only 2 unique numbers in  $V_1(\mathbb{R}^3)$ .

We remark that the procedure described above can also be understood as an implementation of Algorithm 1.2, a dimensionality reduction on Grassmannian manifolds rather than Stiefel manifolds, in the following way. Consider the commutative diagram below, where the vertical maps are the natural quotient maps,  $\alpha$  is as in Algorithm 1.1, and  $\bar{\alpha}$  is naturally induced on the associated quotient spaces.

$$(5.1) \quad \begin{array}{ccc} V_1(\mathbb{R}^3) & \xrightarrow{\alpha} & V_1(\mathbb{R}^{83}) \\ \downarrow & & \downarrow \\ Gr(1, \mathbb{R}^3) & \xrightarrow{\bar{\alpha}} & Gr(1, \mathbb{R}^{83}) \end{array}$$

For each point  $y$  in our data set  $Y$  of 24 PSD matrices, we consider its largest eigenvalue  $\lambda(y)$  and associated eigenspace  $E_{\lambda(y)}$ , which is an element of  $Gr(1, \mathbb{R}^{83})$ . Selecting a particular

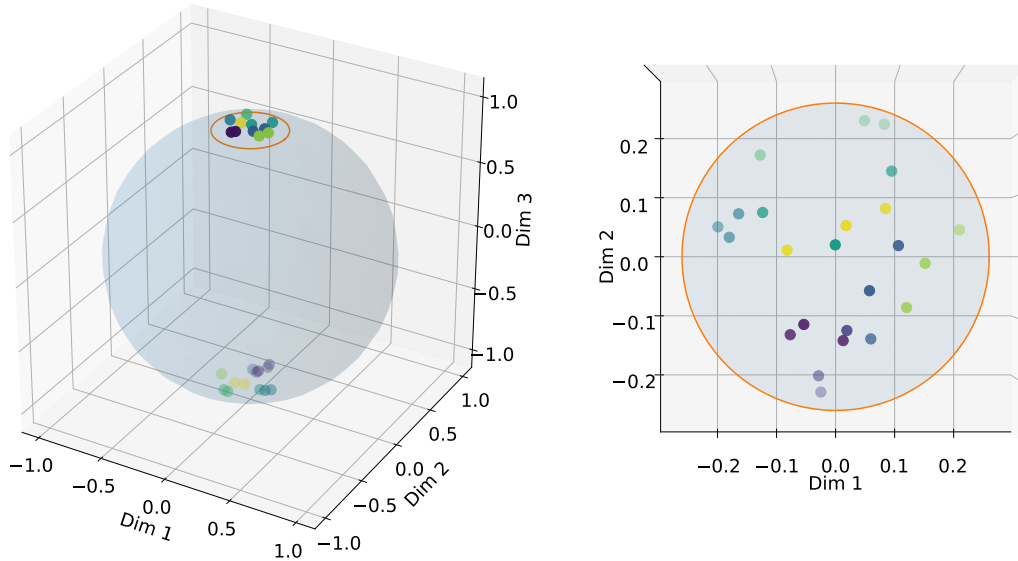


**Figure 5.4.** Left: 24 brain connectivity matrices projected from  $\mathbb{R}^{83 \times 83}$  to  $V_1(\mathbb{R}^{83})$  to  $V_1(\mathbb{R}^3)$ , colored by their corresponding eight human subjects. Right: Zoomed-in and birds-eye view of the data after all points in the lower hemisphere are reflected across the  $z = 0$  plane to the upper hemisphere.

unit-length eigenvector from each eigenspace is well-defined only up to multiplication by  $-1$ , and constitutes a “lift” of  $E_{\lambda(y)}$  to an element  $\tilde{y}$  of  $V_1(\mathbb{R}^{83})$ . Then, we perform Algorithm 1.1 to obtain data in  $V_1(\mathbb{R}^3)$  (left hand of Figure 5.4) and finally project to  $Gr(1, \mathbb{R}^3)$  (right hand of Figure 5.4).

**5.4. Application to a stimulus space model.** In this section, we discuss an application of our methodology to data arising from neuroscience. Many neural phenomena can be effectively analyzed using a *stimulus space model* [2, 6, 8, 20, 31]. This model supposes the existence of an underlying metric stimulus space  $(S, d_S)$  and assigns neurons  $\{1, 2, \dots, k\}$  in a population to points  $\{n_1, n_2, \dots, n_k\}$  in  $S$ . Then, a stimulus is modeled as a time-series  $\{s_1, s_2, \dots, s_N\}$  of points in  $S$ . In general, a neuron’s response to a stimulus decreases with distance. Thus, the response  $r_i(s_k)$  of neuron  $i$  to stimulus  $s_k$  can be described by

$$(5.2) \quad r_i(s_k) = f_i(d_S(n_i, s_k))$$

where  $f_i$  is some (usually unknown) monotonically decreasing function.

A central problem in modern computational neuroscience is to extract information about the stimulus space or the stimulus itself from the activity of the encoding neurons alone. The fact that the response functions  $f_i$  are unknown, highly nonlinear, and often vary with time means that standard linear methods are often of limited use.

In many observed systems, the underlying stimulus space has an inherent and nontrivial topology. For instance, head direction [4, 19, 36] and orientation in visual cortex [2] can be modeled by circular stimulus spaces. In the case when the stimulus space is fully sampled,

persistence techniques can be used to decode topological information about the stimulus [28]. See also [18], [30, Section 6], and [29, Section 6].

We simulate the case of a circular stimulus space that has been only partially sampled. For instance, while head direction can often be well-described with circular coordinates, limited range of motion (e.g., looking roughly 90 degrees to the left and right) means that the associated circular stimulus space may only be sampled from, for instance, 0 to  $\pi$ . In this case, methods as in [28] will be ineffective as they require detecting a high-persistence feature of the data, such as a “full” circle, using persistent cohomology.

In further detail, we consider a population  $\{1, 2, \dots, 100\}$  of 100 neurons identified with uniformly distributed points  $\{n_1, n_2, \dots, n_{100}\}$  on a half-circle, from 0 to  $\pi$ . Each neuron  $n_i$  is assigned a response function

$$(5.3) \quad f_i = \max(1 - m_i x, 0)$$

where the slope  $m_i$  is chosen uniformly randomly between 25 and 50.

We simulated neural activity in response to a stimulus modeled by a random walk  $\{t_1, t_2, \dots, t_{13,000}\}$  on the half-circle comprising 13,000 steps. Activity of the neural population at step  $t_i$  can be recorded as vector with 100 entries, one for each neuron. Thus, the collective activity over the whole time series can be encoded as a point cloud in  $\mathbb{R}^{100}$  with  $N = 13,000$  points.

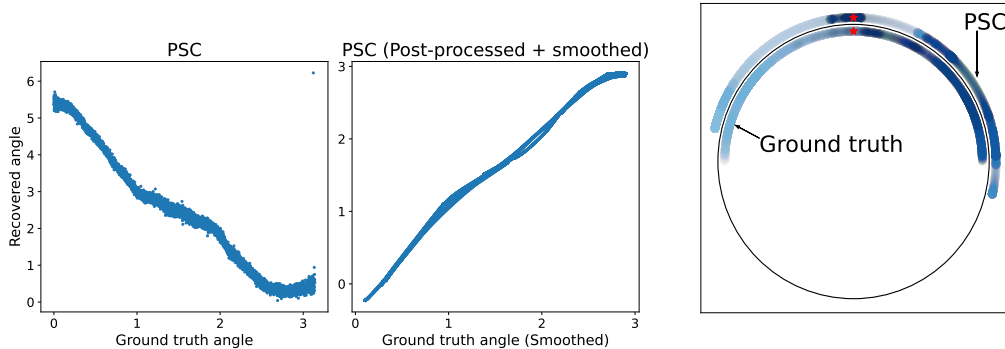


**Figure 5.5.** *Left: Angular coordinates of a geometric walk on a half-circle against coordinates recovered via PSC from neural response. Middle: Post-processed and smoothed recovered coordinates against smoothed ground truth angles. Right: Angles plotted on a circle. Smoothed ground truth angles are plotted in the inner circle, while the post-processed and smoothed PSC angles are in the outer ring. PSC angles are shifted to align with ground truth angle at  $t = 0$  (red stars). Color intensity correlates with time steps.*

First, we centered the data by subtracting the neural population’s average response from each entry. Then, we normalized the data to obtain a point cloud on  $S^{99}$ . Hypothesizing that the neural stimulus (i.e., random walk) could be well-approximated by a time series on a half-circle, we ran Algorithm 1.1 with  $n = 1$ . In Figure 5.5, we compare the recovered data on  $S^1$  to the ground truth coordinates of the random walk as in [7, Section 3].

The takeaway of Figure 5.5 is that our method accurately recovers the neural stimulus up to rotation and scaling, each of which can easily be addressed in post-processing with knowledge

of the spatio-temporal relationship of a few points of the ground truth input. Indeed, after 1) uniformly rotating the recovered coordinates so that the recovered coordinate of the initial time step matched that of the ground truth, and 2) scaling the recovered coordinates, we recover the stimulus (i.e., random walk on the half-circle) almost exactly. Figure 5.6 shows the recovered walk with no post-processing (top right) and with post-processing (bottom right) as well as the ground truth walk with and without Gaussian smoothing (top and bottom left, respectively).

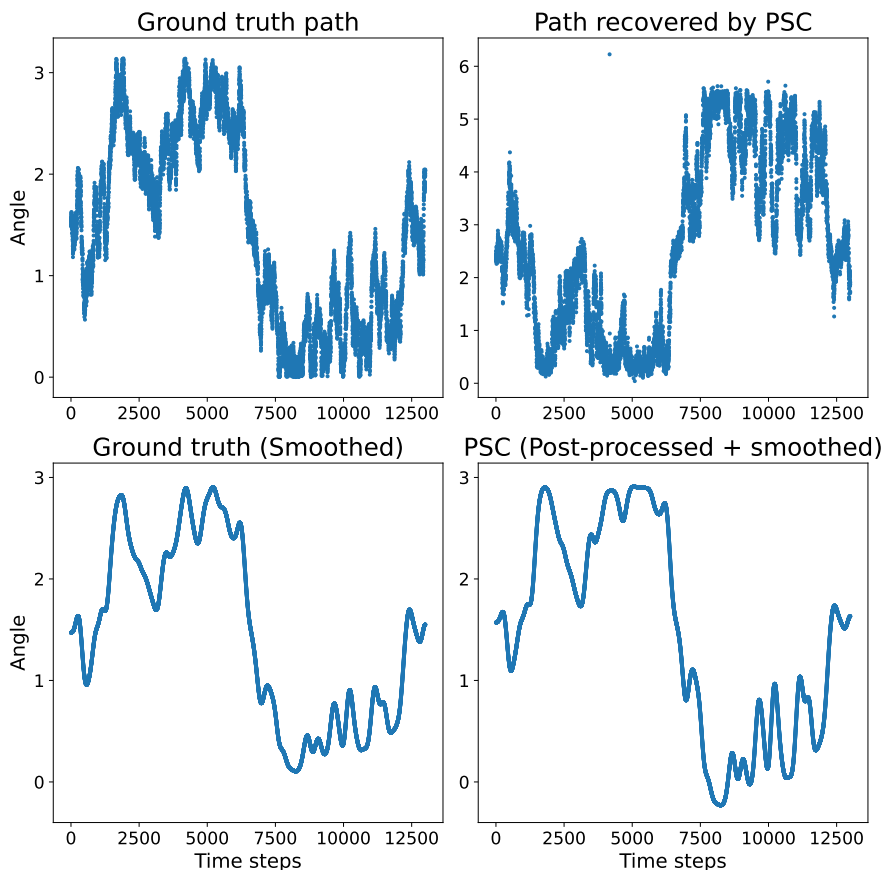


**Figure 5.6.** *Ground truth recovered time series (top left), recovered time series with no post-processing (top right), smoothed ground truth time series (bottom left), and smoothed, post-processed recovered time series (bottom right).*

By contrast, existing methods such as multidimensional scaling or persistent cohomology fail to accurately recover the input stimulus from the recorded neural response. Figure 5.7 shows the analogue of Figure 5.5 but using multidimensional scaling (top left, limited to 150 iterations to avoid excessive computation time) and persistent cohomology (top right) on the same centered and normalized data set and with the same axes, namely, ground truth versus recovered angle. For the persistence approach, we computed the persistent cohomology of the 100-dimensional point cloud and used the circular coordinates algorithm of [25] to

extract a map from the data to  $S^1$  from the longest-lived (though still very short) persistent cohomology class. Lastly, this example also highlights the importance of choosing the “right”  $\alpha$  as described in Algorithm 1.1. Figure 5.7 also shows coordinate recovery using a random  $\alpha$  (bottom left) and  $\alpha_{PCA}$  (bottom right). Using a random  $\alpha$  clearly yields poor recovery and while  $\alpha_{PCA}$  accurately recovers some points, there is notable improvement using  $\alpha_{GD}$ .

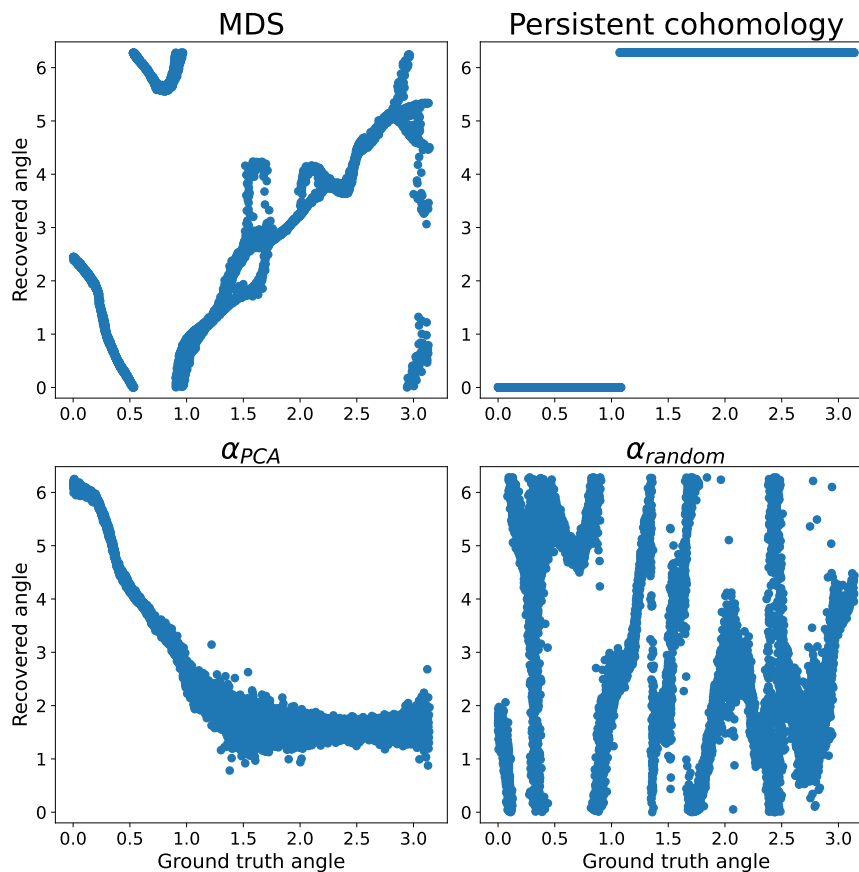


**Figure 5.7.** Angular coordinates of ground truth stimulus vs. recovered coordinates from MDS (top left), persistent cohomology (top right), with  $\alpha_{PCA}$  (bottom left), and with a random  $\alpha$  (bottom right).

**Acknowledgments.** This material is based upon AMS Mathematics Research Communities (MRC) work supported by the National Science Foundation under Grant Number DMS-1916439.

H. Lee’s work was partially completed while the author was at Department of Mathematics, University of California Los Angeles, and was partially supported by NSF DMS-1952339.

J. A. Perea’s work was partially supported by the National Science Foundation through grants CCF-2006661, and CAREER award DMS-1943758.

N. Schonscheck’s work is supported by the Air Force Office of Scientific Research under award FA9550-21-1-0266. This author also wishes to thank Chad Giusti for his continued support.

## REFERENCES

- [1] S. ATASOY, I. DONNELLY, AND J. PEARSON, *Human brain networks function in connectome-specific harmonic waves*, Nature communications, 7 (2016), p. 10340.
- [2] R. BEN-YISHAI, R. L. BAR-OR, AND H. SOMPOLINSKY, *Theory of orientation tuning in visual cortex.*, Proceedings of the National Academy of Sciences, 92 (1995), pp. 3844–3848, <https://doi.org/10.1073/pnas.92.9.3844>.
- [3] I. CHAMI, A. GU, D. NGUYEN, AND C. RÉ, *Horopca: Hyperbolic dimensionality reduction via horospherical projections*, (2021).
- [4] R. CHAUDHURI, B. GERÇEK, B. PANDEY, A. PEYRACHE, AND I. FIETE, *The intrinsic attractor manifold and population dynamics of a canonical cognitive circuit across waking and sleep*, Nature Neuroscience, 22 (2019), pp. 1512–1520, <https://doi.org/10.1038/s41593-019-0460-x>.
- [5] Y. CHIKUSE, *Statistics on Special Manifolds*, Lecture Notes in Statistics, Springer New York, 2012, <https://books.google.com/books?id=71X1BwAAQBAJ>.
- [6] M. M. CHURCHLAND, J. P. CUNNINGHAM, M. T. KAUFMAN, J. D. FOSTER, P. NUYUJUKIAN, S. I. RYU, AND K. V. SHENOY, *Neural population dynamics during reaching*, Nature, 487 (2012), pp. 51–56, <https://doi.org/10.1038/nature11129>.
- [7] V. DE SILVA, D. MOROZOV, AND M. VEJDEMO-JOHANSSON, *Persistent Cohomology and Circular Coordinates*, Discrete & Computational Geometry, 45 (2011), pp. 737–759, <https://doi.org/10.1007/s00454-011-9344-x>.
- [8] S. DENEVE, P. E. LATHAM, AND A. POUGET, *Reading population codes: A neural implementation of ideal observers*, Nature Neuroscience, 2 (1999), pp. 740–745, <https://doi.org/10.1038/11205>.
- [9] I. L. DRYDEN, K.-R. KIM, C. A. LAUGHTON, AND H. LE, *Principal nested shape space analysis of molecular dynamics data*, The Annals of Applied Statistics, 13 (2019), pp. pp. 2213–2234, <https://www.jstor.org/stable/26866721> (accessed 2023-08-17).
- [10] K. FAN AND A. J. HOFFMAN, *Some metric inequalities in the space of matrices*, Proc. Amer. Math. Soc., 6 (1955), pp. 111–116, <https://doi.org/10.2307/2032662>, <https://doi-org.udel.idm.oclc.org/10.2307/2032662>.
- [11] X. FAN, C. YANG, AND B. C. VEMURI, *Nested hyperbolic spaces for dimensionality reduction and hyperbolic nn design*, in 2022 IEEE/CVF Conference on Computer Vision and Pattern Recognition (CVPR), Los Alamitos, CA, USA, jun 2022, IEEE Computer Society, pp. 356–365, <https://doi.org/10.1109/CVPR52688.2022.00045>, <https://doi.ieeecomputersociety.org/10.1109/CVPR52688.2022.00045>.
- [12] P. T. FLETCHER, C. LU, S. M. PIZER, AND S. JOSHI, *Principal geodesic analysis for the study of nonlinear statistics of shape*, IEEE transactions on medical imaging, 23 (2004), pp. 995–1005.
- [13] G. H. GOLUB AND C. F. VAN LOAN, *Matrix computations*, The Johns Hopkins University Press, 1996.
- [14] N. J. HIGHAM, *Functions of matrices*, Society for Industrial and Applied Mathematics (SIAM), Philadelphia, PA, 2008, <https://doi.org/10.1137/1.9780898717778>, <https://doi-org.udel.idm.oclc.org/10.1137/1.9780898717778>. Theory and computation.
- [15] S. JUNG, I. L. DRYDEN, AND J. S. MARRON, *Analysis of principal nested spheres*, Biometrika, 99 (2012), pp. 551–568, <https://doi.org/10.1093/biomet/ass022>, <https://doi.org/10.1093/biomet/ass022>, <https://arxiv.org/abs/https://academic.oup.com/biomet/article-pdf/99/3/551/17461502/ass022.pdf>.
- [16] P. JUPP AND K. MARDIA, *Directional Statistics*, Wiley, 2000.
- [17] W. KAHAN, *The nearest orthogonal or unitary matrix*, August 2011. <https://people.eecs.berkeley.edu/~wkahan/Math128/NearestQ.pdf>.
- [18] L. KANG, B. XU, AND D. MOROZOV, *Evaluating state space discovery by persistent cohomology in the spatial representation system*, Frontiers in Computational Neuroscience, 15 (2021), <https://doi.org/10.3389/fncom.2021.616748>, <https://www.frontiersin.org/articles/10.3389/fncom.2021.616748>.
- [19] S. S. KIM, H. ROUAULT, S. DRUCKMANN, AND V. JAYARAMAN, *Ring attractor dynamics in the Drosophila central brain*, Science, 356 (2017), pp. 849–853, <https://doi.org/10.1126/science.aal4835>.
- [20] V. MANTE, D. SUSSILLO, K. V. SHENOY, AND W. T. NEWSOME, *Context-dependent computation by recurrent dynamics in prefrontal cortex*, Nature, 503 (2013), pp. 78–84, <https://doi.org/10.1038/nature12742>.
- [21] C. MANTOUX, B. COUVY-DUCHESNE, F. CACCIAMANI, S. EPELBAUM, S. DURRLEMAN, AND S. ALLAS-

- SONNIÈRE, *Understanding the variability in graph data sets through statistical modeling on the stiefel manifold*, Entropy, 23 (2021), p. 490.
- [22] N. MIOLANE, N. GUIGUI, A. L. BRIGANT, J. MATHE, B. HOU, Y. THANWERDAS, S. HEYDER, O. PELTRE, N. KOEP, H. ZAATITI, H. HAJRI, Y. CABANES, T. GERALD, P. CHAUCHAT, C. SHEWMAKE, D. BROOKS, B. KAINZ, C. DONNAT, S. HOLMES, AND X. PENNEC, *Geomstats: A python package for riemannian geometry in machine learning*, Journal of Machine Learning Research, 21 (2020), pp. 1–9, <http://jmlr.org/papers/v21/19-027.html>.
- [23] S. F. MULDOON, F. PASQUALETTI, S. GU, M. CIESLAK, S. T. GRAFTON, J. M. VETTEL, AND D. S. BASSETT, *Stimulation-based control of dynamic brain networks*, PLoS computational biology, 12 (2016), p. e1005076.
- [24] J. A. PEREA, *Multiscale projective coordinates via persistent cohomology of sparse filtrations*, Discrete & Computational Geometry, 59 (2018), pp. 175–225.
- [25] J. A. PEREA, *Sparse Circular Coordinates via Principal  $\mathbb{Z}$ -Bundles*, in Topological Data Analysis, N. A. Baas, G. E. Carlsson, G. Quick, M. Szymik, and M. Thauale, eds., Abel Symposia, Cham, 2020, Springer International Publishing, pp. 435–458, [https://doi.org/10.1007/978-3-030-43408-3\\_17](https://doi.org/10.1007/978-3-030-43408-3_17).
- [26] L. POLANCO AND J. A. PEREA, *Coordinatizing data with lens spaces and persistent cohomology*, in Proceedings of the 31st Canadian Conference on Computational Geometry (CCCG), 2019, pp. 49–57.
- [27] D. RAMÍREZ, I. SANTAMARÍA, AND L. SCHARF, *Subspace averaging and its applications*, in Coherence: In Signal Processing and Machine Learning, Springer, 2022, pp. 259–296.
- [28] E. RYBAKKEN, N. BAAS, AND B. DUNN, *Decoding of Neural Data Using Cohomological Feature Extraction*, Neural Computation, 31 (2019), pp. 68–93, [https://doi.org/10.1162/neco.a\\_01150](https://doi.org/10.1162/neco.a_01150).
- [29] N. C. SCHONSHECK AND S. C. SCHONSHECK, *Spherical coordinates from persistent cohomology*, To appear in Journal of Applied and Computational Topology, (2023), <https://arxiv.org/abs/2209.02791>.
- [30] L. SCOCCOLA, H. GAKHAR, J. BUSH, N. SCHONSHECK, T. RASK, L. ZHOU, AND J. A. PEREA, *Toroidal Coordinates: Decorrelating Circular Coordinates with Lattice Reduction*, in 39th International Symposium on Computational Geometry (SoCG 2023), E. W. Chambers and J. Gudmundsson, eds., vol. 258 of Leibniz International Proceedings in Informatics (LIPIcs), Dagstuhl, Germany, 2023, Schloss Dagstuhl – Leibniz-Zentrum für Informatik, pp. 57:1–57:20, <https://doi.org/10.4230/LIPIcs.SoCG.2023.57>, <https://drops.dagstuhl.de/opus/volltexte/2023/17907>.
- [31] H. S. SEUNG AND H. SOMPOLINSKY, *Simple models for reading neuronal population codes.*, Proceedings of the National Academy of Sciences of the United States of America, 90 (1993), pp. 10749–10753.
- [32] A. ŠKOCH, B. REHÁK BUČKOVÁ, J. MAREŠ, J. TINTĚRA, P. SANDA, L. JAJCAY, J. HORÁČEK, F. ŠPANIEL, AND J. HLINKA, *Human brain structural connectivity matrices—ready for modelling*, Scientific Data, 9 (2022), p. 486.
- [33] J. TIAN, J. ZHAO, AND C. ZHENG, *Clustering of cancer data based on stiefel manifold for multiple views*, BMC bioinformatics, 22 (2021), pp. 1–15.
- [34] J. TOWNSEND, N. KOEP, AND S. WEICHWALD, *Pymanopt: A python toolbox for optimization on manifolds using automatic differentiation*, Journal of Machine Learning Research, 17 (2016), p. 1–5, <http://jmlr.org/papers/v17/16-177.html>.
- [35] P. TURAGA, A. VEERARAGHAVAN, A. SRIVASTAVA, AND R. CHELLAPPA, *Statistical computations on grassmann and stiefel manifolds for image and video-based recognition*, IEEE Transactions on Pattern Analysis and Machine Intelligence, 33 (2011), pp. 2273–2286.
- [36] D. TURNER-EVANS, S. WEGENER, H. ROUAULT, R. FRANCONVILLE, T. WOLFF, J. D. SEELIG, S. DRUCKMANN, AND V. JAYARAMAN, *Angular velocity integration in a fly heading circuit*, eLife, 6 (2017), p. e23496, <https://doi.org/10.7554/eLife.23496>.
- [37] C.-H. YANG AND B. C. VEMURI, *Nested grassmannians for dimensionality reduction with applications*, Machine Learning for Biomedical Imaging, 1 (2022), pp. 1–21, <https://doi.org/https://doi.org/10.59275/j.melba.2022-234f>, <https://melba-journal.org/2022:002>.